Distinct yet Overlapping Functions of VMP1 and TMEM41B in Modulating Hepatic Lipoprotein Secretion and Autophagy in MASH

Allen Chen[1], Khue Nguyen[1], Xiaoxiao Jiang[1], Xiaochen Yu[1], Yan Xie[2], Wanqing Liu[3], Nicholas O. Davidson[2], Wen-Xing Ding[1,4], Hong-Min Ni[1*]

1. Department of Pharmacology, Toxicology and Therapeutics, University of Kansas Medical Center, Kansas City, KS, USA;
2. Division of Gastroenterology, Department of Medicine, Washington University School of Medicine, St. Louis, MO, USA;
3. Department of Pharmaceutical Sciences, Wayne State University, Detroit, MI, USA
4. Department of Internal Medicine, University of Kansas Medical Center, Kansas City, KS, USA;

*Correspondence to: Hong-Min Ni, MD., Department of Pharmacology, Toxicology and Therapeutics, University of Kansas Medical Center, MS 1018, 3901 Rainbow Blvd., Kansas City, Kansas 66160. Tel: 913-588-8999. Email: hni@kumc.edu

Key Words: Endoplasmic reticulum, liver injury, MASLD, steatosis, VLDL.

Electronic word count:

Number of figures and tables: 8

Financial support: The research was supported in part by NIDDK R01 DK129234 (to H-M. Ni), NIAAA R37AA020518, R01AA031230 (to W-X. Ding), DK119437, HL151328 and DDRCC P30 DK052574 (to N.O. Davidson), National Institute of General Medical Sciences of COBRE grant P20GM144269 (to S. Weinman), and Allen Chen was partially supported by T32 DK128770.

Conflict of interest: The authors participating in this study declare that they have nothing to disclose.

Author's contributions: AC. performed experiments, data analysis and interpretation and preparation of manuscript; KN., XJ., XY., and WXD. performed experiments, data analysis and interpretation; WL, NOD. and WXD. assisted in data interpretation and contributed to the writing of the manuscript; HMN. supervised the project, participated in research design, performed experiments, data analysis and interpretation, and wrote the manuscript. All authors read and approved the final manuscript.

Abbreviations: AAV, adeno-associated virus; ADRP, adipose differentiation related protein; ALT, alanine aminotransferase; α-SMA, alpha smooth muscle actin; Col1a1, collagen, type-1,alpha-1; CDAHFD, choline-deficient, amino acid-defined HFD (45 % fat) containing 0.1% methionine; COPII, coat protein complex II; CTGF, connective tissue growth factor; ER, endoplasmic reticulum; FFA, free fatty acid; FPLC, Fast protein liquid chromatography; H&E, hematoxylin and eosin; IL-1β, Interleukin-1 beta; IL-10, Interleukin-10; KI, knockin; KO, knockout; LD, lipid droplet; MAM, mitochondrial associated membrane; MTTP, microsomal triglyceride transfer protein; MASLD, metabolic dysfunction-associated steatotic liver disease; MASH, metabolic dysfunction-associated steatohepatitis; PC, phosphatidylcholine; PDI, protein disulfide isomerase; PE, phosphatidylethanolamine; PEMT, Phosphatidylethanolamine N-methyltransferase; PISD, phosphatidylserine decarboxylase ; PL, phospholipid; RIPA, radioimmunoprecipitation; SREBP, sterol regulatory element-binding protein; TBG, thyroxine binding globulin; TG, triglyceride; TGF1β, transforming growth factor 1 beta 1; VMP1, vacuole membrane protein 1; WT, wild-type; 1.

Abstract

Background: Transmembrane protein 41B (TMEM41B) and vacuolar membrane protein 1 (VMP1) are endoplasmic reticulum (ER) transmembrane scramblase proteins that have been recently identified to have important roles in autophagy and hepatic lipoprotein secretion. While TMEM41B and VMP1 are structurally and functionally similar, the nature of their interactions and how they coordinately regulate hepatic lipoprotein secretion and autophagy in metabolic-associated steatotic liver disease (MASLD) and metabolic-associated steatohepatitis (MASH) remains unclear.

Methods: Liver-specific and hepatocyte-specific *Tmem41b* knockout (KO) mice as well as *Tmem41b* knock-in (KI) mice were generated from *Tmem41b*^{flox} or *Tmem41b*^{KI} mice by crossing with albumin-Cre mice or by injecting AAV8-TBG-cre, respectively. Lipid metabolism in these mice was characterized by lipidomic analyses. Mice with hepatic overexpression of TMEM41B that were fed a MASH diet were also characterized. To explore the relationship between TMEM41B and VMP1, *Tmem41b/Vmp1* double KO (DKO), *Tmem41b* KO/*Vmp1* KI, and *Vmp1* KO/*Tmem41b* KI mice were generated, and steatosis and autophagy were characterized.

Results: The loss of hepatic *Tmem41b* severely impaired very low-density lipoprotein (VLDL) secretion, resulting in significant microsteatosis, increased hepatic triglycerides, inflammation, fibrosis, and ultimately the MASH development. TMEM41B protein was decreased in human MASLD livers. Overexpression of TMEM41B mitigated the effects of diet-induced MASLD. Mice lacking both *Vmp1* and *Tmem41b* (DKO) showed further impairment in VLDL secretion compared to single *Tmem41b* KO, but were similar that of *Vmp1* KO mice. Lipidomic analysis of liver tissues revealed decreased levels of phosphatidylcholine and phosphatidylethanolamine, along with increased neutral lipids. Cellular fractionation studies indicated that VMP1 and TMEM41B localize at the mitochondrial-associated membrane (MAM). Electron microscopy analysis showed reduced contact between mitochondria and the ER in hepatocytes deficient in

either VMP1 or TMEM41B. The loss of hepatic VMP1 or TMEM41B led to markedly increased levels of LC3B-II and p62/SQSTM1, which were not further affected by double deletion of VMP1 and TMEM41B. Restoring VMP1 in *Tmem41b* KO mice partially improved defective VLDL secretion, though autophagy was only partially corrected by overexpression of VMP1 at a low but not high level. In contrast, restoring TMEM41B in *Vmp1* KO mice dose-dependently improved both defective VLDL secretion and autophagy.

Conclusion: Loss of hepatic VMP1 or TMEM41B decreases MAM and phospholipid content and reduces VLDL secretion, resulting in the development of MASH. TMEM41B and VMP1 may have overlapping but distinct mechanisms in regulating lipoprotein secretion and autophagy.

.

Introduction

Metabolic dysfunction-associated steatotic liver disease (MASLD) has become the most common chronic liver disease globally, affecting an estimated 24% of the population and having limited FDA-approved pharmacotherapies [1]. Left untreated, MASLD can progress to metabolic dysfunction-associated steatohepatitis (MASH), which is defined by hepatocyte death and inflammation in the setting of steatosis. Unaddressed, MASH can precipitate the development of end-stage liver diseases, including cirrhosis and hepatocellular carcinoma.

Research into MASLD/MASH treatment commonly focuses on upregulating hepatic lipid catabolism or blocking absorption of lipids from the gut, thus decreasing overall systemic lipid levels [2]. Previous studies have identified vacuolar membrane protein 1 (VMP1) as an endoplasmic reticulum (ER) resident transmembrane protein with important roles in regulating the formation of autophagosomes and lipid droplets [3-5]. VMP1 is required for normal hepatic VLDL secretion, which is decreased in diet-induced MASH mouse livers and in human MASH livers. Genetic ablation of VMP1 leads to rapid hepatic steatosis and decreased serum triglyceride levels. Conversely, VMP1 overexpression alleviated diet-induced steatosis by enhancing VLDL secretion [5].

Transmembrane Protein 41B (TMEM41B), another ER-resident transmembrane protein, has been identified to have similar roles to VMP1, specifically as an important mediator of autophagy and lipid homeostasis [6-8]. While both *Tmem41b* and *Vmp1* single knock-out (KO) are able to cause rapid hepatic steatosis due to VLDL secretion defect [3, 9], whether VMP1 and TMEM41B serve the exact same roles within the hepatocytes in VLDL secretion regulation and MASLD development are unknown. Moreover, it remains unclear whether VMP1 and TMEM41B may be able to compensate for the other in regulating VLDL secretion and autophagy.

Here, we examine levels of TMEM41B expression in human MASH livers and further investigate the role of TMEM41B and its relationship with VMP1 in regulating lipid homeostasis, autophagy, and VLDL secretion in mouse livers. Our findings provide novel insights into the molecular relationship between VMP1 and TMEM41B as well as the mechanisms involved in VLDL secretion. Additionally, we propose that VMP1 and TMEM41B could serve as potential targets for treating MASLD and MASH.

Materials and Methods

Animals

The *Vmp1*^{flox} and *Vmp1* conditional knockin (KI) mice were described previously [5]. The *Tmem41b*^{flox} and *Tmem41b* conditional KI mice were generated in collaboration with Cyagen (Santa Clara, CA). Briefly, to generate *Tmem41b*^{flox} mice, ES cells containing *Tmem41b* exons 3-5 cassette which were flanked by two loxP sequences. Cre-mediated depletion of exons 3-5 leads to a frameshift, resulting in a small truncated peptide. To generate *Tmem41b* conditional KI mice, ES cells containing an insertion of *Tmem41b-3×Flag* cassette which contains a polyA tail flanked by two *loxP* sequences between CAG promoter and *Tmem41b-3×Flag* under *Rosa26* loci were injected into C57BL/6N blastocysts to obtain chimeric mice. The chimeric mice were crossed with C57BL/6N to obtain mutant mice. Cre-mediated depletion of the polyA tail leads to expression of TMEM41b-FLAG. *Tmem41b*^{flox,} *Vmp1*^{flox} mice were generated by crossing *Tmem41b*^{flox} with *Vmp1*^{flox} mice. *Tmem41b* ^{flox}, *Vmp1*^{KI} mice were generated by crossing *Tmem41b*^{flox} mice with *Vmp1*^{KI} mice. *Vmp1*^{flox}, *Tmem41b*^{KI} mice were generated by crossing *Vmp1*^{flox} mice with *Tmem41b*^{KI} mice. To generate liver-specific KO/KI mice, the mutant mice were crossed with albumin-Cre mice. To generate hepatocyte-specific *Tmem41b* (H-*Tmem41b)* KO mice, *Tmem41b*^{flox} were injected intravenously with adeno-associated virus 8 (AAV8)-thyroxine binding globulin promoter (TBG)-null or AAV8-TBG-cre (1×10^{11} GC/mouse). All mice were fed with a chow diet unless otherwise indicated. To generate a model of diet-induced MASH, mice were fed a CDAHFD (choline-deficient, amino acid-defined high-fat diet (45% fat) containing 0.1% methionine) for 6 weeks. Mice were specific pathogen-free and maintained in a barrier rodent facility under standard experimental conditions. All procedures were approved by the Institutional Animal Care and Use Committee of the University of Kansas Medical Center.

Reagents and antibodies

Antibodies and reagents used in this study are listed in the supplementary table 1.

Hepatic triglyceride (TG) and cholesterol analysis

Hepatic lipid extraction was performed as described previously[10]. Briefly, frozen liver tissues (20-50 mg) were homogenized and followed by lipid extraction using a chloroform-methanol mixture. The resulting lipid extracts were analyzed for TG and cholesterol content using the GPO-Triglyceride Reagent Set and Cholesterol liquid reagent (catalog #T7532 and #C7510, Pointe Scientific, Canton, MI), following the manufacturer's protocols.

***In vivo* VLDL secretion assay**

In vivo VLDL secretion assay was performed as previously described[11]. Mice were subjected to a 4-hour fast prior to the intraperitoneal administration of Pluronic™ F-127 at a dosage of 10 mg/kg. Pluronic™ F-127 inhibits both the lipolysis and the tissue uptake of lipoproteins in mice. Blood samples were collected at baseline (pre-injection) and subsequently at hourly intervals for a duration of 3 hours post-injection. TG concentrations were quantified using the colorimetric assay described above.

Blood Biochemistry analysis

Serum TG and cholesterol levels were quantified using the colorimetric assays outlined above. Serum alanine aminotransferase (ALT) activity was assessed using commercially available kit (catalog #A7526, Pointe Scientific) in accordance with the manufacturer's instructions.

Histology and immunohistochemistry analysis

Livers were preserved in 10% neutral buffered formalin and subsequently embedded in paraffin. Sections of 5 μm thickness from the paraffin blocks were stained using hematoxylin and eosin (H&E) for histopathological assessment. For immunohistochemical analysis, F4/80 was utilized

to identify macrophages, while Sirius Red staining was employed to visualize collagen deposition.

Oil Red O staining

Oil Red O staining was performed using liver cryo-sections as described previously[12]. Livers were preserved in 4% paraformaldehyde overnight at 4ºC, then infiltrated with 20% sucrose overnight at the same temperature, and embedded in Tissue-Tek OCT Compound. Sections of 6 μm thickness were stained with Oil Red O in 60% isopropanol for 15 minutes at 37ºC. This was followed by a wash with 60% isopropanol and three washes with water, then stained with hematoxylin, concluding with a final wash with water.

Electron microscopy analysis

Electron microscopy was performed as described previously[13]. Breifly, livers were perfused with 2.5% glutaraldehyde in a 0.1M sodium cacodylate buffer and subsequently sectioned into small fragments. Ultra-thin sections were then stained with uranyl acetate and lead citrate. Imaging was performed using a JEM 1016CX electron microscope (JEOL) to analyze the ultrastructural details.

Immunoblot analysis

Liver proteins were extracted using RIPA buffer, containing 1% NP40, 0.5% sodium deoxycholate, and 0.1% sodium dodecyl sulfate (SDS) in phosphate-buffered saline (PBS). A total of 30 μg of protein was separated on an SDS-PAGE gel, followed by transfer onto a PVDF membrane. The membranes were subsequently incubated with appropriate primary antibodies, followed by corresponding secondary antibodies, and detection was performed using SuperSignal Plus chemiluminescent substrate (Thermo Fisher Scientific). Densitometric analysis of the bands was conducted using ImageJ or Un-Scan-It software, with normalization to β-actin or GAPDH. All densitometry data are reported as mean ± SEM.

Quantitative real-time polymerase chain reaction

RNA was extracted from murine hepatic tissue using Trizol reagent (Thermo Fisher Scientific) and subsequently reverse transcribed into complementary DNA (cDNA) utilizing RevertAid H minus reverse transcriptase (Thermo Fisher Scientific) [14]. Quantitative real-time PCR was conducted on a Bio-Rad CFX384™ detection system employing SYBR® Green mix (Bimake, Houston, TX). Expression of *Acta2, Adgre, Cd68, Col1a1, Ctgf, Il1b, Il10, Tgfb1, and Trem2* was quantified using qRT-PCR analysis and *Actb* was used as an internal control. The fold change of mRNA was expressed as $2^{-\Delta\Delta Ct}$.

Lipidomics analysis

Lipidomic profiling of mouse liver tissues was conducted at Metabolon, Inc. (Durham, NC) as described previously [5]. Briefly, for lipidomic analysis, lipids were extracted from samples in a methanol:dichloromethane mixture in the presence of internal standards. After concentration under nitrogen, the lipid extracts were reconstituted in 0.25 mL of 10 mM ammonium acetate dichloromethane:methanol (50:50). These extracts were subsequently transferred to inserts and loaded into vials for infusion mass spectrometry (MS) analysis, utilizing a Shimadzu LC equipped with nano PEEK tubing and the Sciex SelexION-5500 QTRAP. The analysis was conducted in both positive and negative ionization modes. The 5500 QTRAP operated in Multiple Reaction Monitoring (MRM) mode, with over 1,100 monitored reactions. Quantification of individual lipid species was achieved by calculating the peak area ratios of the target lipids to their corresponding internal standards, which were then normalized to the known concentrations of the internal standards added during extraction. Lipid class concentrations were derived as the aggregate of all molecular species within each class, while fatty acid profiles were delineated by determining the constituency of each class based on individual fatty acids. Statistical evaluations were conducted using ArrayStudio, R (http://cran.r-project.org/), or JMP, with

significance assessed via one-way ANOVA. The false discovery rate (FDR) was estimated utilizing q-values to adjust for multiple comparisons.

Subcellular fractionation

Subcellular fractionation was performed using an adapted, previously described protocol [15]. Mouse livers from 1-month-old LWT, *Tmem41b*^{LKO} and *Vmp1*^{LKO} mice were homogenized in a mannitol-sucrose-BSA-EGTA-Tris buffer using a Potter-Elvehjem tissue homogenizer. Mitochondria were separated from cytosolic fractions through a series of 9,000g-10,000g centrifugations. Following this, 95,000g-100,000g centrifugations in 30% vol/vol Percoll solution was performed to separate MAM from mitochondria. ER was isolated from cytosolic fractions after subjecting the supernatant from a 20,000g centrifugation to a 100,000g centrifugation then collecting pellet. Subcellular fractions were subsequently performed using immunoblot analysis.

Statistical analysis

Data were analyzed in R or with GraphPad. All experimental data are expressed as mean ± SEM and subjected to unpaired Student's *t test* (2 group comparisons) or one-way ANOVA with post-hoc Turkey test (multigroup comparisons).

Results

Hepatic deletion of TMEM41B impairs lipoprotein secretion and leads to rapid development of microvesicular Steatosis

To investigate the physiological functions of TMEM41B in mice, 8-week-old *Tmem41b*^{flox} mice were injected with a single dose of AAV8-TBG-Cre (hepatocyte-specific *Tmem41b* KO, *Tmem41b*^{HKO}) or AAV8-TBG-Null (hepatocyte wild-type (HWT)) for 2 and 4 weeks. Compared to HWT mice, *Tmem41b*^{HKO} mice had enlarged and pale livers with significant increases in liver-body weight ratio (**Fig. 1A**). Hematoxylin and Eosin (H&E) staining revealed pan-hepatic microvesicular steatosis in *Tmem41b*^{HKO} mice (**Fig. 1B**). Hepatic triglyceride (TG) and cholesterol were significantly elevated in *Tmem41b*^{HKO} mice compared with HWT mice (**Fig. 1C**). Accordingly, serum TG and cholesterol levels were significantly decreased post-AAV injection (**Fig. 1D**). We next performed lipoprotein secretion analysis in *Tmem41b*^{HKO} and HWT mice. Compared with HWT mice, serum TG was markedly decreased in *Tmem41b*^{HKO} mice in a time-dependent manner with Pluronic™ F-127 administration to inhibit lipolysis and tissue uptake of TG-rich lipoproteins. TG secretion rate was reduced by 81.55% in *Tmem*41b^{HKO} mice (**Fig. 1E**). Immunoblot analysis showed decreased serum apolipoprotein (APO)B100 in *Tmem41b*^{HKO} (**Fig. 1F**). Fast protein liquid chromatography (FPLC) analysis demonstrated substantially decreased VLDL-TG levels in *Tmem41b*^{HKO} mice without affecting peak change (**Fig. 1G**), confirming impaired VLDL secretion in *Tmem41b*^{HKO} mice.

Like *Tmem41b*^{HKO} mice, one-month-old liver-specific*Tmem41b* KO (*Tmem41b*^{LKO}) mice also showed hepatomegaly (**Fig. S1A**), massive steatosis (**Fig. S1B**), markedly increased hepatic TG and cholesterol contents (**Fig. S1C**), and decreased serum TG and cholesterol (**Fig. S1D**). VLDL secretion and APOB100 were also decreased in *Tmem41b*^{LKO} mice (**Fig. S1E**). TG secretion rate was reduced by 65.81% in *Tmem41b*^{LKO} mice (**Fig. S1E**). Notably, like male mice, female *Tmem41b*^{HKO} mice developed a similar increase in liver-body weight ratio, hepatic TG

and cholesterol, and a decrease in serum TG and cholesterol (**Fig. S2A-2D**). These data indicate that TMEM41B plays an important role in regulating hepatic VLDL secretion and lipid homeostasis in mice.

Hepatic deletion of TMEM41B leads to the development of MASH

Serum levels of ALT increased in *Tmem41b*^{HKO} and *Tmem41b*^{LKO} mice (**Fig. 2A, Fig. S1F**). Hepatic mRNA levels of inflammatory genes were markedly increased in *Tmem41b*^{HKO} mice (**Fig. 2B**). F4/80-positive macrophages also increased in *Tmem41b*^{HKO} mice (**Fig. 2C**). *Tmem41b*^{HKO} mice displayed increased liver Sirius Red staining at 10 weeks post AAV injection (**Fig. 2D**). Hepatic mRNA levels of fibrotic genes and protein levels of α-smooth muscle actin were elevated in *Tmem41b*^{HKO} mice as early as 2 weeks post AAV injection compared to matched WT mice (**Fig. 2E-F**). Together, these data indicate that hepatic deletion of *Tmem41b* leads to MASH in mice.

Decreased TMEM41B is associated with human MASLD livers and overexpression of TMEM41B alleviates diet-Induced hepatic steatosis

To examine whether TMEM41B is associated with human MASLD, protein levels of TMEM41B in human normal, steatosis, and MASH livers were analyzed. Immunoblot analysis revealed that TMEM41B levels significantly declined in human steatosis and histology-confirmed MASH livers (**Fig. 3A-B**). Mice fed with CDAHFD (choline-deficient, amino acid-defined HFD (45 % fat) containing 0.1% methionine), a MASH diet, also had decreased hepatic TMEM41B (**Fig. 3C**). To examine the therapeutic effect of TMEM41B in CDAHFD-induced steatosis, conditional *Tmem41b* knockin mice were established and fed with CDAHFD (**Fig. 3D**). Overexpression of TMEM41B alleviated CDAHFD-induced steatosis (**Fig. 3E**), liver/body weight ratio enlargement and hepatic TG accumulation (**Fig. 3F**). Overexpression of TMEM41B also restored decreased TMEM41B caused by CDAHFD in mouse livers without affecting VMP1 levels (**Fig. 3G**).

Hepatic deletion of *Tmem41b* or *Vmp1* leads to decreased hepatic levels of phospholipids and disrupts ER-mitochondria contact

Unbiased lipodomics analysis revealed that hepatic levels of metabolites in the phosphatidylcholines (PC) and phosphatidylethanolamines (PE) metabolism pathways decreased significantly in *Tmem41b*^{HKO} or *Vmp1*^{HKO} mouse livers. In contrast, neutral lipids, including cholesteryl esters (CE), diacyl- and triacylglycerols were significantly increased in *Tmem41b*^{HKO} or *Vmp1*^{HKO} mouse livers (**Fig. 4A**).

ER- Mitochondria contact sites are critical for phospholipid synthesis and calcium transport [16]. EM analysis revealed that ER-Mitochondria contact sites were readily detected in HWT, *Tmem41b*^{LKO}, and *Vmp1*^{LKO} mouse hepatocytes (**Fig. 4B**). ER-Mitochondria contact sites were graded based on a 4-point scale to assess the contact between ER and mitochondria, with Grade 1 being minimal contact (<25%) and Grade 4 indicating mitochondria nearly completely enveloped by ER (>75%). These quantitative EM analysis results showed fewer ER-Mitochondria contact sites in *Tmem41b*^{LKO} or *Vmp1*^{LKO} mouse hepatocyte than WT hepatocytes (**Fig. 4C**). These data suggest disruption of the ER-mitochondria interaction with loss of TMEM41B or VMP1 (**Fig. 4B**).

To delve into the possible effects of *Tmem41b* or *Vmp1* KO on ER-mitochondria contact, cell fractionation was performed using livers from hepatic *Tmem41b* or *Vmp1* KO and their WT littermates. Both TMEM41B and VMP1 were enriched at the ER and mitochondrial-associated membrane (MAM) (**Fig. 4D**). Phosphatidylethanolamine N-methyltransferase (PEMT) and phosphatidylserine decarboxylase (PISD) are two enzymes important for PC and PE synthesis. While PEMT was enriched at the ER and MAM with higher levels on MAM in WT mouse livers, *Tmem41b*^{LKO} or *Vmp1*^{LKO} mice had reduced total PEMT and PEMT in MAM fractions (**Fig. 4D**). PISD was only located on mitochondria with no change or slight decrease in hepatic level in *Tmem41b*^{LKO} or *Vmp1*^{LKO} mice (**Fig. 4D**). VMP1 protein level was reduced at MAM in

Tmem41b^{LKO} mouse livers. Conversely, loss of VMP1 led to a profound decrease in TMEM41B localization to MAM sites. However, considerable levels of TMEM41B were detected in the ER fraction of *Tmem41b*^{LKO} mouse livers, which could be from non-parenchymal cells. To our surprise, a trace of VMP1 was observed on mitochondria fractions and need further investigation.

Knockout of both *Tmem41b* and *Vmp1* does not further exacerbate impaired lipoprotein secretion and hepatic steatosis

To further assess the relationship between TMEM41B and VMP1 in regulating VLDL secretion, hepatic *Tmem41b* /*Vmp1* double KO (DKO) mice were generated. DKO mice developed steatosis and hepatomegaly, which were comparable to that of either *Tmem41b*^{LKO} or *Vmp1*^{LKO} mice (**Fig. 5A-C**). *Vmp1*^{LKO} and DKO mice had similar serum ALT that was slightly higher than that of *Tmem41b*^{LKO} mice (**Fig. 5C**). *Vmp1*^{LKO} and DKO mice had more severe VLDL secretion defect compared to defect in *Tmem41b*^{LKO} mice. TG secretion rate was reduced by 49.44%, 62.88%, and 69.38%, respectively, in *Tmem41b*^{LKO} and *Vmp1*^{LKO}, and DKO mice (**Fig. 5D**).

Microsomal triglyceride transfer protein (MTTP) and disulfide isomerase (PDI), required for VLDL assembly, were slightly increased in *Tmem41b*^{LKO} and DKO but not in *Vmp1*^{LKO} mice (**Fig 5E**). While several COPII proteins, SEC23A, SEC24A, and SEC24D, required for exit of VLDL from ER, were moderately reduced in *Vmp1*^{LKO} mouse livers, their protein levels were profoundly reduced in either *Tmem41b*^{LKO} or *DKO* mouse livers (**Fig. 5E**). Interestingly, while loss of TMEM41B did not change VMP1 protein levels, loss of VMP1 profoundly decreased TMEM41B protein in mouse livers (**Fig. 5E**). PEMT and PISD were profoundly decreased in *Vmp1*^{LKO} mouse livers, which was not further decreased in DKO livers (**Fig. 5F**). These results indicate that TMEM41B and VMP1 may have different impacts on the machinery proteins regulating VLDL secretion.

Overexpression of hepatic VMP1 partially alleviated steatosis caused by the loss of TMEM41B

Overexpression of VMP1 significantly improved pale liver color in *Tmem41b*^{LKO} mice and reduced microsteatosis, as observed through H&E staining of liver sections. There was no notable difference in steatosis improvement between heterozygous and homozygous overexpression of VMP1 (**Fig. 6A-B**). Additionally, both heterozygous and homozygous overexpression of VMP1 partially corrected elevated levels of serum ALT and liver-to-body weight ratio in *Tmem41b*^{LKO} mice (**Fig. 6C**). Overexpression of VMP1 also resulted in a significant reduction of hepatic TG and cholesterol in *Tmem41b*^{LKO} mice, regardless of whether VMP1 was overexpressed heterozygously or homozygously (**Fig. 6D**).

Overexpression of hepatic TMEM41B improved VLDL secretion and partially alleviated Steatosis caused by the loss of VMP1

The effect of TMEM41B restoration in *Vmp1*^{LKO} mice was investigated. Overexpression of TMEM41B in *Vmp1*^{LKO} mice alleviated steatosis as demonstrated by H&E staining of liver sections (**Fig. 7A-B**). Overexpression of TMEM41B also partially corrected increased liver body weight ratio and serum levels of ALT in *Vmp1*^{LKO} mice (**Fig. 7C**). Levels of hepatic TG and cholesterol were also reversed with overexpression of TMEM41B in *Vmp1*^{LKO} mice (**Fig. 7D**). Notably, homozygous Tmem41b KI mice had much better improvement than heterozygous Tmem41b KI mice for the above parameters in *Vmp1*^{LKO} mice. The restoration of TMEM41B in *Vmp1*^{LKO} mice also improved VLDL secretion. TG secretion rate was reduced by 69.87% in *Vmp1*^{LKO} mice but improved by 21.7% with TMEM41B overexpression (**Fig. 7E**).

Overexpression of TMEM41B in *Vmp1*^{LKO} and VMP1 in *Tmem41b*^{LKO} mice partially corrects autophagy defect

Consistent with previous findings [17], immunoblot analysis showed that levels of LC3B-II and p62 were increased in *Tmem41b*^{HKO} mouse livers (**Fig. 8A**), indicating impaired autophagy by deletion of *Tmem41b*. The levels of LC3-II and p62 were comparable in *Vmp1*^{LKO} *and DKO* mice but were much higher than those of *Tmem41b*^{LKO} mice (**Fig. 8B**), suggesting VMP1 may be more critical than TMEM41B in regulating autophagy in mouse livers.

Heterozygous overexpression of VMP1 slightly corrected increased levels of hepatic LC3-II but not p62 in *Tmem41b*^{LKO} mouse livers (**Fig. 8C**). Homozygous overexpression of VMP1 further increased LC3B-II and p62 **(Fig. 8C)**. Levels of LC3B-II and p62 were increased in *Vmp1*^{LKO} mouse livers. Heterozygous overexpression of TMEM41B partially corrected increased levels of hepatic LC3-II and p62 in *Vmp1*^{LKO} mouse livers which were further corrected by homozygous overexpression of TMEM41B (**Fig. 8D**). These results suggest that TMEM41B and VMP1 may have different impacts in regulating hepatic autophagy.

Discussion

In this study, we found that *Vmp1*^{LKO} mice developed more severe VLDL secretion defects than Tmem41b^{LKO} mice, and that hepatic deletion of both *Vmp1* and *Tmem41b* did not further impair VLDL secretion. Furthermore, overexpression of *Vmp1* in *Tmem41b*-deficient mouse livers only partially alleviated steatosis; yet, overexpression of *Tmem41b* in *Vmp1*-deficient mouse livers improved VLDL and ameliorated steatosis in a dose-dependent manner. Moreover, hepatic deletion of *Tmem41b* reduces VMP1 protein levels, and *vice versa*. In addition to VLDL secretion, overexpression of TMEM41B partially corrected autophagy defects in VMP1 LKO mice dose-dependently, whereas overexpression of low but not high levels of VMP1 corrected autophagy defects in TMEM41B LKO mice. These data indicate that VMP1 and TMEM41B have similar yet distinct roles in regulating hepatic VLDL secretion and autophagy. Previous studies that compared predicted structures of TMEM41B and VMP1 have identified sequence homology between these two proteins. Notably, both VMP1 and TMEM41B contain a DedA domain consisting of 2 transmembrane helices and one extramembrane helix along with 2 reentrant loops. TMEM41B and VMP1 seem to structurally differ primarily with respect to their N terminuses, in which TMEM41B contains fewer transmembrane domains but an extramembrane domain not present in VMP1 [18, 19].

LDs are cytosolic organelles that store metabolic energy and consist of a hydrophobic core of neutral lipids surrounded by a phospholipid monolayer decorated with proteins. Using EM analysis, a previous study showed that TMEM41B-deficient hepatocytes lack mature lipoproteins; instead, LDs were encapsulated by highly curved ER membranes [9]. However, EM analysis and immunofluorescence staining of ER and neutral lipids revealed that LDs in *Vmp1* KO hepatocytes are either partially or completely enclosed within the ER membrane bilayer, suggesting that VMP1 is required for the neutral lipids to bud off the ER membrane bilayer and enter the ER lumen [5, 20]. Nonetheless, 3D EM analysis is needed to further

determine the difference and the exact location of LDs in VMP1- and TMEM41B-deficient hepatocytes.

Three processes critical for VLDL secretion occur at specific ER sites. These include (1) import of neutral lipids from the ER bilayer into the ER lumen, (2) assembly of pre-VLDL in the ER lumen, and (3) export of pre-VLDL from the ER lumen. It is known that MTTP is required to transfer the bulk of triglycerides into APOB100 at the ER lumen for VLDL assembly. Deletion of MTTP abolishes VLDL secretion. MTTP activity is enhanced by PDI, which is regulated by the IRE1α-XBP1s-PDI axis, decreased IRE1α-mediated PDI production impairing hepatic VLDL secretion in mice [21-23]. Pre-VLDL particles are progressively lipidated, which require MTTP and other players, including TM6SF2 [24]. Liver-specific *Tm6sf2* KO mice exhibit steatosis and reduced VLDL secretion with small and underlipidated VLDL particles without affecting APOB secretion. We did not find significant changes in either hepatic MTTP or PDI in *Tmem41b* or *Vmp1* KO hepatocytes, suggesting that alteration in MTTP and PDI are less likely to contribute to steatosis in these KO mice. Assembly of pre-VLDL in the ER lumen is APOB-dependent [25]. We found that hepatic APOB100 levels markedly decreased in hepatic *Tmem41b* or *Vmp1* KO mouse livers and serum, which may indicate preferential impacts on pre-VLDL assembly in the ER lumen impairing VLDL secretion [26]. It has been reported that TMEM41B and VMP1 directly interacted with APOB100 [9, 20]. TMEM41B seems to be an important regulator of COPII-coated vesicle transport at the ER exit sites, particularly with respect to SEC23A. It is known that the COPII-coated vesicle is assembled through a signaling pathway beginning with SAR1 and SURF4 and progressing through SEC proteins. It has been reported that TMEM41B interact with SURF4 at ER exit sites to assist in COP-II-coated vesicle formation [9]. VMP1 also interacted with SEC24D and substantially colocalized with SEC24D in hepatocytes of mouse livers. It is likely that TMEM41B and VMP1 may increase the stability of APOB and COPII complex proteins [5]. Future studies are needed to dissect how TMEM41B and VMP1 might

regulate hepatic APOB and COPII proteins either at the posttranslational level, transcriptional level, or both. Notably, it has been reported that VMP1 and TMEM41B interact with each other. [17]. As deletion of VMP1 decreased TMEM41B levels, TMEM41B and VMP1 potentially stabilize each other within hepatocytes.

ER membrane phospholipid content and composition are critical for ER membrane remodeling, curvature and tension, which are also important for LD budding from the ER bilayer [27, 28]. The amount of PC and PE as well as the fatty acyl chain compositions of PC and PE, especially PC and PE arachidonyl chain, has been shown to regulate VLDL secretion [29, 30]. The decreased hepatic PC and PE content, together with the changes to the acyl-chain composition of phospholipids in *Tmem41b*- or *Vmp1*-deficienct hepatocytes may thus change the biophysical tension and curvature of the ER membrane, arresting import of neutral lipids from the ER membrane bilayer to the ER lumen. *Vmp1*-deficienct hepatocytes have a more profound PL decrease than *Tmem41b*-deficient hepatocytes, which may explain the more severe impairment of VLDL secretion in VMP1 LKO mice than in TMEM41B LKO mice. ER-mitochondria contact sites are critical for PL transfer. We found that *Tmem41b*- or *Vmp1*-deficiency hepatocytes have decreased ER-mitochondria contact sites. Furthermore, both TMEM41B and VMP1 are located at MAM, and PEMT and PISD, two important PL synthesis enzymes, were reduced in *Tmem41b*- and/or *Vmp1*-deficient livers. Decreased PEMT and PISD may contribute to reduced PL synthesis. Several studies also showed that TMEM41B and VMP1 are ER scramblases, which may affect PL distribution [3, 18, 31]. Both TMEM41B and VMP1 possess a DedA domain and were structurally predicted to serve as half transporters for ion and lipid transport [32]. Future work is needed to investigate whether and how TMEM41B and VMP1 directly interact with PEMT and PISD to regulate the synthesis of PC and PE. Whether the DedA domain of TMEM41B and VMP1 may affect equilibration of PL in the ER bilayer and contribute to VLDL secretion defect remains to be fully investigated.

In addition to their function in VLDL secretion, TMEM41B and VMP1 also regulate autophagy at an early step likely by promoting autophagosome closure [17, 33, 34]. Like in a previous report [17], we found autophagy defect to be more severe in VMP1^{LKO} mouse livers than in TMEM41B^{LKO} livers. Hepatic deletion of both TMEM41 and VMP1 did not further exacerbate impaired autophagy. We also found that low level VMP1 overexpression partially corrected autophagy defect in VMP1-deficient mouse livers. However, high level VMP1 overexpression impaired autophagy in TMEM41B-deficient mouse livers, suggesting that too much VMP1 may also impair autophagy, though the mechanisms behind this hormesis dose response need to be further studied in the future. TMEM41B could correct autophagy defects in VMP1^{LKO} mouse livers in a dose-dependent manner, which is different from findings from a previous report using cultured HEK293 cells [17]. It is likely that the fine-tuned levels of TMEM41B and VMP1 in mouse hepatocytes in vivo could be different from that of cultured HEK293 cells. Notably, several *in vitro* studies showed that VMP1 deficiency causes an increase in membrane contact sites such as ER-mitochondria, ER-endosomes, ER-lipid droplets, and ER-autophagosomes through VAP-mediation or other mechanisms, suggesting that VMP1 inhibits contact site formation in HeLa, COS7 and MEF cells [4, 34, 35]. In contrast to VMP1, the involvement of TMEM41B in membrane contact has not been well investigated. We and others found that ER-mitochondria contact sites or perhaps total ER were reduced in *Tmem41b*- or *Vmp1*-deficient hepatocytes [5, 9]. It seems that organelle contact regulation by VMP1 and TMEM41B may be cell type dependent. However, how TMEM41B and VMP1 regulate ER-mitochondria and other organelle contact sites, along with their roles in regulating autophagy, needs further investigation.

A recent report identified rare and low-frequency ATG7 loss-of-function variants that promote MASLD progression by impairing autophagy and facilitating ballooning and inflammation in the European population [36]. Increased cell death, inflammation, and fibrosis have been observed

in hepatic Atg5 and Atg7-deficiency mice, which have impaired autophagy, but not impaired VLDL secretion and steatosis [34]. However, most genetically modified mouse MASLD models, such as hepatic *Surf4-, Lpcat3-* , *Mea6-* , and *Sar1b*-deficiency mice, showed defective hepatic VLDL secretion and hepatic steatosis, though none of them developed MASH [29, 37-39]. Therefore, the MASH phenotypes in VMP1 and TMEM41B KO mice are distinct from these MASLD models. The MASH phenotypes in *Vmp1* and *Tmem41b* KO mice are likely due to combined impaired VLDL secretion and autophagy, which is unique to TMEM41B and VMP1.

In summary, we found that human MASH livers have decreased hepatic VMP1 and TMEM41B. Our results indicate that lack of hepatic TMEM41B and VMP1 impair both VLDL secretion and autophagy, resulting in MASH in mice. Overexpression of VMP1 alleviates steatosis but not autophagy at high expression level whereas overexpression of TMEM41B improves VLDL secretion, ameliorates steatosis, and partially corrects autophagy defects. It is likely that TMEM41B and VMP1 have both redundant and distinct roles in regulating VLDL secretion and autophagy, and future studies designed to boost hepatic TMEM41B but not VMP1 may be beneficial in enhancing VLDL secretion and improving MASH pathology in humans.

ACKNOWLEDGEMENTS

The authors acknowledge Liver Center for human liver samples. The authors also thank KUMC Electron Microscopy Research Lab facility for assistance with the transmission electron microscope.

References

1. Younossi, Z.M., et al., *Global epidemiology of nonalcoholic fatty liver disease-Meta-analytic assessment of prevalence, incidence, and outcomes.* Hepatology, 2016. **64**(1): p. 73-84.
2. Ipsen, D.H., J. Lykkesfeldt, and P. Tveden-Nyborg, *Molecular mechanisms of hepatic lipid accumulation in non-alcoholic fatty liver disease.* Cell Mol Life Sci, 2018. **75**(18): p. 3313-3327.
3. Li, Y.E., et al., *TMEM41B and VMP1 are scramblases and regulate the distribution of cholesterol and phosphatidylserine.* J Cell Biol, 2021. **220**(6).
4. Reinisch, K.M., X.W. Chen, and T.J. Melia, *"VTT"-domain proteins VMP1 and TMEM41B function in lipid homeostasis globally and locally as ER scramblases.* Contact (Thousand Oaks), 2021. **4**.
5. Jiang, X., et al., *Lack of VMP1 impairs hepatic lipoprotein secretion and promotes non-alcoholic steatohepatitis.* J Hepatol, 2022. **77**(3): p. 619-631.
6. Hoffmann, H.H., et al., *TMEM41B Is a Pan-flavivirus Host Factor.* Cell, 2021. **184**(1): p. 133-148 e20.
7. Kratzel, A., et al., *A genome-wide CRISPR screen identifies interactors of the autophagy pathway as conserved coronavirus targets.* PLoS Biol, 2021. **19**(12): p. e3001490.
8. Schneider, W.M., et al., *Genome-Scale Identification of SARS-CoV-2 and Pan-coronavirus Host Factor Networks.* Cell, 2021. **184**(1): p. 120-132 e14.
9. Huang, D., et al., *TMEM41B acts as an ER scramblase required for lipoprotein biogenesis and lipid homeostasis.* Cell Metab, 2021. **33**(8): p. 1655-1670 e8.
10. Ma, X., et al., *Loss of hepatic DRP1 exacerbates alcoholic hepatitis by inducing megamitochondria and mitochondrial maladaptation.* Hepatology, 2023. **77**(1): p. 159-175.
11. Li, Y., et al., *Impaired Fasting-Induced Adaptive Lipid Droplet Biogenesis in Liver-Specific Atg5-Deficient Mouse Liver Is Mediated by Persistent Nuclear Factor-Like 2 Activation.* Am J Pathol, 2018. **188**(8): p. 1833-1846.
12. Chao, X., et al., *Persistent mTORC1 activation due to loss of liver tuberous sclerosis complex 1 promotes liver injury in alcoholic hepatitis.* Hepatology, 2023. **78**(2): p. 503-517.
13. Wang, S., et al., *Critical Role of TFEB-Mediated Lysosomal Biogenesis in Alcohol-Induced Pancreatitis in Mice and Humans.* Cell Mol Gastroenterol Hepatol, 2020. **10**(1): p. 59-81.
14. Chao, X., et al., *Impaired TFEB-Mediated Lysosome Biogenesis and Autophagy Promote Chronic Ethanol-Induced Liver Injury and Steatosis in Mice.* Gastroenterology, 2018. **155**(3): p. 865-879 e12.
15. Wieckowski, M.R., et al., *Isolation of mitochondria-associated membranes and mitochondria from animal tissues and cells.* Nat Protoc, 2009. **4**(11): p. 1582-90.
16. Voeltz, G.K., et al., *Making the connection: How membrane contact sites have changed our view of organelle biology.* Cell, 2024. **187**(2): p. 257-270.
17. Morita, K., et al., *Genome-wide CRISPR screen identifies TMEM41B as a gene required for autophagosome formation.* J Cell Biol, 2018. **217**(11): p. 3817-3828.
18. Chen, A., W.X. Ding, and H.M. Ni, *Scramblases as Regulators of Autophagy and Lipid Homeostasis: Implications for NAFLD.* Autophagy Rep, 2022. **1**(1): p. 143-160.
19. Hama, Y., H. Morishita, and N. Mizushima, *Regulation of ER-derived membrane dynamics by the DedA domain-containing proteins VMP1 and TMEM41B.* EMBO Rep, 2022: p. e53894.
20. Morishita, H., et al., *A critical role of VMP1 in lipoprotein secretion.* Elife, 2019. **8**.

21. Wang, S., et al., *IRE1alpha-XBP1s induces PDI expression to increase MTP activity for hepatic VLDL assembly and lipid homeostasis.* Cell Metab, 2012. **16**(4): p. 473-86.
22. Newberry, E.P., et al., *Liver-specific deletion of Mttp versus Tm6sf2 reveals distinct defects in stepwise VLDL assembly.* J Lipid Res, 2021. **62**: p. 100080.
23. Raabe, M., et al., *Analysis of the role of microsomal triglyceride transfer protein in the liver of tissue-specific knockout mice.* J Clin Invest, 1999. **103**(9): p. 1287-98.
24. Newberry, E.P., et al., *Liver-Specific Deletion of Mouse Tm6sf2 Promotes Steatosis, Fibrosis, and Hepatocellular Cancer.* Hepatology, 2021. **74**(3): p. 1203-1219.
25. Davidson, N.O. and G.S. Shelness, *APOLIPOPROTEIN B: mRNA editing, lipoprotein assembly, and presecretory degradation.* Annu Rev Nutr, 2000. **20**: p. 169-93.
26. Kulinski, A., S. Rustaeus, and J.E. Vance, *Microsomal triacylglycerol transfer protein is required for lumenal accretion of triacylglycerol not associated with ApoB, as well as for ApoB lipidation.* J Biol Chem, 2002. **277**(35): p. 31516-25.
27. Ben M'barek, K., et al., *ER Membrane Phospholipids and Surface Tension Control Cellular Lipid Droplet Formation.* Dev Cell, 2017. **41**(6): p. 591-604 e7.
28. Fei, W., et al., *A role for phosphatidic acid in the formation of "supersized" lipid droplets.* PLoS Genet, 2011. **7**(7): p. e1002201.
29. Rong, X., et al., *Lpcat3-dependent production of arachidonoyl phospholipids is a key determinant of triglyceride secretion.* Elife, 2015. **4**.
30. Hashidate-Yoshida, T., et al., *Fatty acid remodeling by LPCAT3 enriches arachidonate in phospholipid membranes and regulates triglyceride transport.* Elife, 2015. **4**.
31. Ghanbarpour, A., et al., *A model for a partnership of lipid transfer proteins and scramblases in membrane expansion and organelle biogenesis.* Proc Natl Acad Sci U S A, 2021. **118**(16).
32. Okawa, F., et al., *Evolution and insights into the structure and function of the DedA superfamily containing TMEM41B and VMP1.* J Cell Sci, 2021. **134**(8).
33. Ding, W.X., et al., *Recent insights about autophagy in pancreatitis.* eGastroenterology, 2024. **2**(2).
34. Zhao, Y.G., et al., *The ER-Localized Transmembrane Protein EPG-3/VMP1 Regulates SERCA Activity to Control ER-Isolation Membrane Contacts for Autophagosome Formation.* Mol Cell, 2017. **67**(6): p. 974-989 e6.
35. Tabara, L.C. and R. Escalante, *VMP1 Establishes ER-Microdomains that Regulate Membrane Contact Sites and Autophagy.* PLoS One, 2016. **11**(11): p. e0166499.
36. Baselli, G.A., et al., *Rare ATG7 genetic variants predispose patients to severe fatty liver disease.* J Hepatol, 2022. **77**(3): p. 596-606.
37. Wang, X., et al., *Receptor-Mediated ER Export of Lipoproteins Controls Lipid Homeostasis in Mice and Humans.* Cell Metab, 2020.
38. Santos, A.J., et al., *TANGO1 and Mia2/cTAGE5 (TALI) cooperate to export bulky pre-chylomicrons/VLDLs from the endoplasmic reticulum.* J Cell Biol, 2016. **213**(3): p. 343-54.
39. Wang, Y., et al., *Mea6 controls VLDL transport through the coordinated regulation of COPII assembly.* Cell Res, 2016. **26**(7): p. 787-804.

Figure Legends

Fig. 1. Hepatic deletion of TMEM41B impairs lipoprotein secretion and leads to rapid development of a micro-vesicular steatosis in mice. (A) Representative images of 8-12-week-old *Tmem41b*^{flox} mice at 4 weeks post AAV8-TBG-null (*Tmem41b*^{HWT}) or AAV8-TBG-cre (*Tmem41b*^{HKO}) injection with liver/body weight ratio. (B) H&E staining of liver tissues from *Tmem41b*^{HWT} and *Tmem41b*^{HKO} mice. Scale bars, 100 μm. Hepatic (C) and serum (D) TG and cholesterol (CHOL) were quantified. (E) *Tmem41b*^{flox} mice at 2 weeks post AAV injection were injected with Pluronic™ F-127 and serum TG concentrations were measured. TG secretion rate was quantified. (F) Serum APOB from *Tmem41b*^{flox} mice at 2 weeks post AAV injection were subjected to immunoblot analysis. (G) Mice were fasted 4 hours followed by Pluronic™ F127 injection for another 3 hours. Serum from the same group of mice was pooled (n=4). Lipoprotein profiles were analyzed by FPLC. *p<0.05, **p<0.01, ***p<0.001, ****p<0.0001 (one-way ANOVA with post-hoc Turkey test (A-D) or unpaired Student's *t test* (E)).

Fig. 2. Hepatic deletion of TMEM41B leads to the development of MASH. (A) Serum ALT in *Tmem41b*^{flox} mice at 2, 4 and 10 weeks post AAV injection. (B) Hepatic mRNA levels of pre-inflammatory cytokines and immune cell marker genes were analyzed by qPCR and normalized to *Actb* mRNA. (C) Immunohistochemistry staining for F4/80 in mouse livers. (D) Sirius Red staining in mouse livers. (E) Hepatic mRNA levels of fibrogenic genes were analyzed by qPCR and normalized to *Actb* mRNA. (F) Immunoblot analysis of α-SMA in mouse livers. Data represent mean ± SEM. *p<0.05, **p<0.01, ***p<0.001, ****p<0.0001 (one-way ANOVA with post-hoc Turkey test).

Fig. 3. Reduced TMEM41B Is associated with human MASLD livers and overexpression of TMEM41B alleviates diet-Induced hepatic steatosis. (A) Immunoblot analysis of TMEM41B and (B) H&E staining in human livers. (C) Protein level of TMEM41B in mice fed with CDAHFD. (D) Scheme of CDAHFD-induced NASH in mice. (E) Representative H&E and Oil O Red

images from mice. Scale bars, 50 μm. (F) Liver-body weight ratio, ALT and hepatic TG in CDAHFD-fed mice. (G) Immunoblot analysis of TMEM41B and VMP1 in mice fed with CDAHFD. Data represent mean ± SEM. * $p<0.05$; **** $p<0.0001$ (one-way ANOVA with post-hoc Turkey test).

Fig. 4. Hepatic deletion of *Tmem41b* or *Vmp1* leads to decline in phospholipids and disrupts ER-mitochondria contact. (A). Heatmap of phospholipids and neutral lipids of mouse livers from *Tmem41b*^{flox} and Vmp1^{flox} mice with AAV8 injection by lipidomics analysis. (B) Representative EM images from *Tmem41b*^{flox} and Vmp1^{flox} mice 2 weeks post AAV8 injection. (C) Representative EM images of HWT, *Tmem41b*^{HKO} and *Vmp1*^{HKO} hepatocytes are shown. White Arrows denote close contact of ER with mitochondria approximately< 30 nm, which are defined as MAM. Red arrows denote damaged mitochondria (M). ER-mitochondria contact sites were quantified in mouse livers and at least 10 images were quantified. Scale bars, 500 nm. (D) Subcellular fractions from 1-month-old LWT, *Tmem41b*^{LKO} and *Vmp1*^{LKO} mice were subjected to immunoblot with the indicated antibodies. Data represent mean ± SEM.

Fig. 5. Knockout of both *Tmem41b* and *Vmp1* does not further exacerbate impaired lipoprotein secretion and hepatic Steatosis. (A) Representative images of 1-month-old WT and DKO mice. (B) H&E staining of liver tissues from the mice. Scale bars, 100 μm. (C) Liver/body weight ratio, ALT, and hepatic TG and cholesterol (CHOL) were measured in mice. (D) LWT, *Tmem41b*^{LKO}, *Vmp1*^{LKO}, and DKO mice were injected with Pluronic™ F-127 and serum TG concentrations were measured. TG secretion rate was quantified. (E) Total liver lysates were extracted from the mice. Total mouse liver lysates were subjected to immunoblot analysis for the indicated proteins and followed by densitometric analysis. (F) PEMT and PISD were examined by immunoblots. Data represent mean ± SEM. *$p<0.05$, ***$p<0.001$, ****$p<0.0001$ (one-way ANOVA with post-hoc Turkey test).

Fig. 6. Overexpression of hepatic VMP1 partially alleviated steatosis caused by the loss of TMEM41B. (A) Representative images of 1-month-old *Tmem41b*^{LKO}, *Tmem41b*^{LKO}/*Vmp1*$^{KI/+}$ and *Tmem41b*^{LKO}/*Vmp1*$^{KI/KI}$ mice. (B) H&E and Oil O Red staining of liver tissues from the mice. Scale bars, 100 μm. (C) Liver/body weight ratio and ALT were measured. (D) Hepatic TG and cholesterol (CHOL) were measured in mice. Data represent mean ± SEM. *p<0.05, **p<0.01, ***p<0.001, ****p<0.0001 (one-way ANOVA with post-hoc Turkey test).

Fig. 7. Overexpression of hepatic TMEM41B improved VLDL secretion and partially alleviated Steatosis caused by the loss of VMP1.

(A) Representative images of 1-month-old *Vmp1*^{LKO}, *Vmp1*^{LKO}/*Tmem41b*$^{KI/+}$ *and* *Vmp1*^{LKO}/*Tmem41b*$^{KI/KI}$ mice. (B) H&E staining of liver tissues from the mice. Scale bars, 100 μm. (C) Liver/body weight ratio and ALT were measured. (D) Hepatic TG and cholesterol (CHOL) were measured in mice. (E) LWT, *Vmp1*^{LKO}, *Vmp1*^{LKO}/*Tmem41b*$^{KI/+}$ *and* *Vmp1*^{LKO}/*Tmem41b*$^{KI/KI}$ mice were injected with Pluronic™ F-127 and serum TG concentrations were measured. VLDL secretion rates were quantified. Data represent mean ± SEM. *p<0.05, **p<0.01, ***p<0.001, ****p<0.0001 (one-way ANOVA with post-hoc Turkey test).

.

Fig. 8. Overexpression of TMEM41B in *Vmp1*^{LKO} and VMP1 in *Tmem41b*^{LKO} mice partially corrects autophagy defect. (A) Total lysates were extracted from *Tmem41b*^{flox} mice at 2 and 4 weeks post AAV injection mice and subjected to the immunoblot analyses with the indicated antibody followed by densitometric analysis. (B) Total lysates were extracted from LWT, *Tmem41b*^{LKO}, *Vmp1*^{LKO}, and DKO mice and subjected to immunoblot analyses with the indicated antibody followed by densitometric analysis. (C) Total lysates were extracted from LWT, *Tmem41b*^{LKO}, *Tmem41b*^{LKO}/*Vmp1*$^{KI/+}$ and *Tmem41b*^{LKO}/*Vmp1*$^{KI/KI}$ mice and subjected to the

immunoblot analyses with the indicated antibody followed by densitometric analysis. (D) Total lysates were extracted from LWT, *Vmp1*^{LKO}, *Vmp1*^{LKO}/*Tmem41b*$^{KI/+}$ *and Vmp1*^{LKO}/*Tmem41b*$^{KI/KI}$ mice and subjected to the immunoblot analyses with the indicated antibody followed by densitometric analysis.

Figure 1

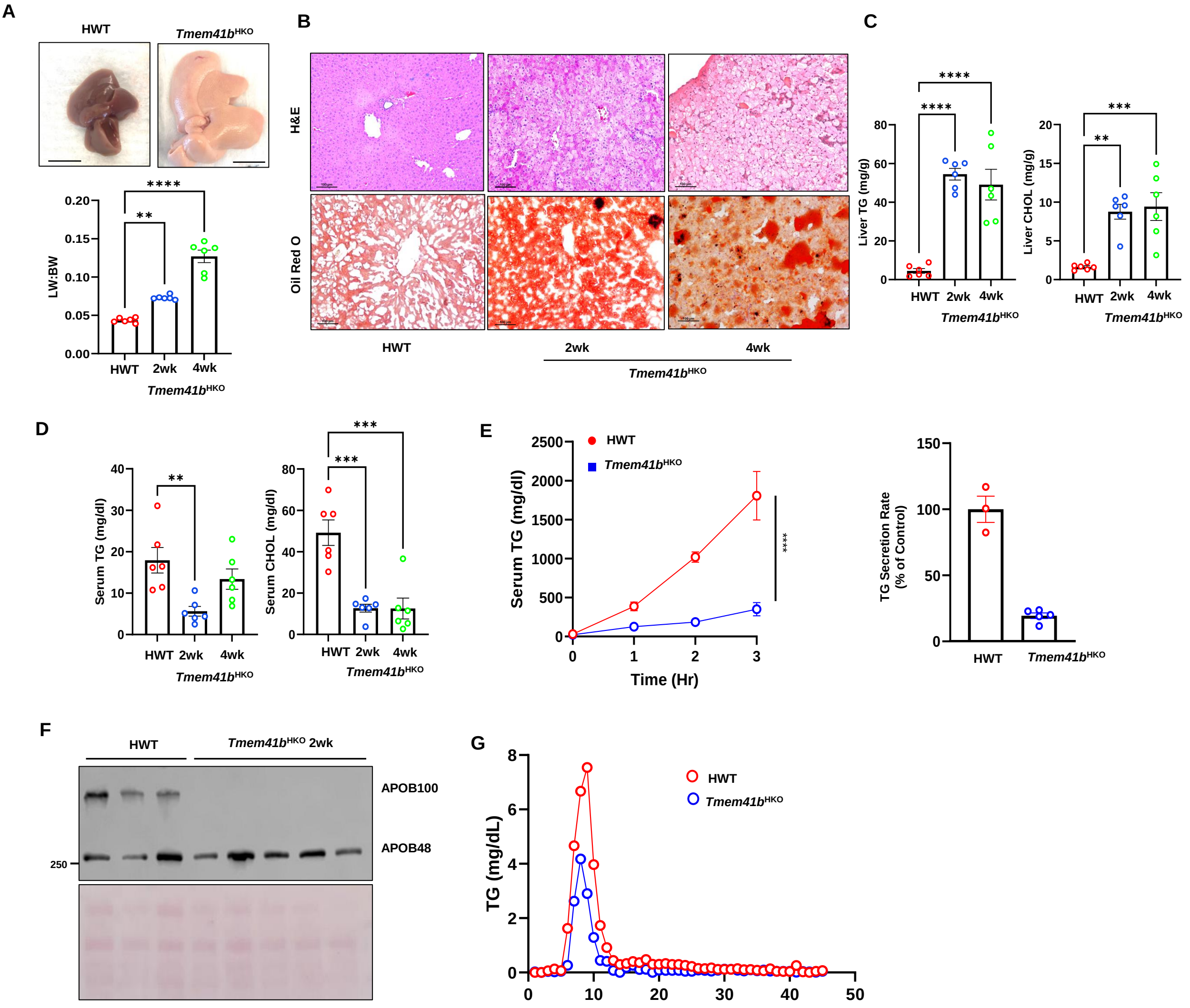
A
HWT
Tmem41b^HKO
LW:BW
0.20
0.15
0.10
0.05
0.00
****
**
HWT
2wk
4wk
Tmem41b^HKO
B
H&E
Oil Red O
HWT
2wk
4wk
Tmem41b^HKO
C
Liver TG (mg/g)
80
60
40
20
0
****
****
HWT
2wk
4wk
Tmem41b^HKO
Liver CHOL (mg/g)
20
15
10
5
0
***
**
HWT
2wk
4wk
Tmem41b^HKO
D
Serum TG (mg/dl)
40
30
20
10
0
**
HWT
2wk
4wk
Tmem41b^HKO
Serum CHOL (mg/dl)
80
60
40
20
0
***
***
HWT
2wk
4wk
Tmem41b^HKO
E
HWT
Tmem41b^HKO
Serum TG (mg/dl)
2500
2000
1500
1000
500
0
****
0
1
2
3
Time (Hr)
TG Secretion Rate (% of Control)
150
100
50
0
HWT
Tmem41b^HKO
F
HWT
Tmem41b^HKO 2wk
APOB100
APOB48
250
G
TG (mg/dL)
8
6
4
2
0
HWT
Tmem41b^HKO
0
10
20
30
40
50

Figure 2

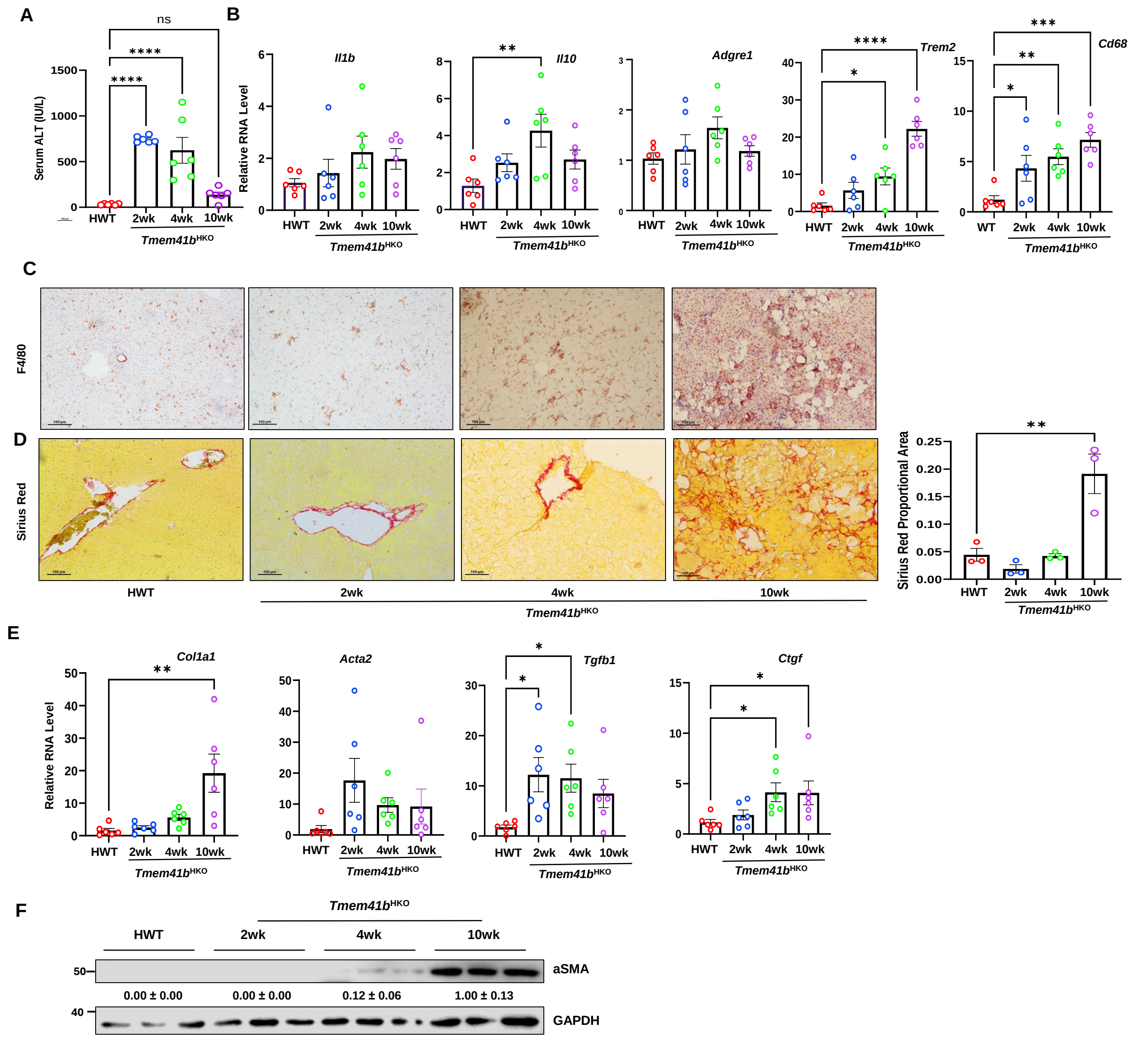
A
ns
****
****
Serum ALT (IU/L)
1500
1000
500
0
HWT
2wk
4wk
10wk
Tmem41b HKO
B
Il1b
Relative RNA Level
Il10
**
Adgre1
Trem2
****
*
Cd68
***
**
*
WT
C
F4/80
D
Sirius Red
HWT
2wk
4wk
10wk
Tmem41b HKO
Sirius Red Proportional Area
0.25
0.20
0.15
0.10
0.05
0.00
E
Col1a1
Acta2
Tgfb1
Ctgf
F
aSMA
GAPDH
0.00 ± 0.00
0.00 ± 0.00
0.12 ± 0.06
1.00 ± 0.13
50
40

Figure 3

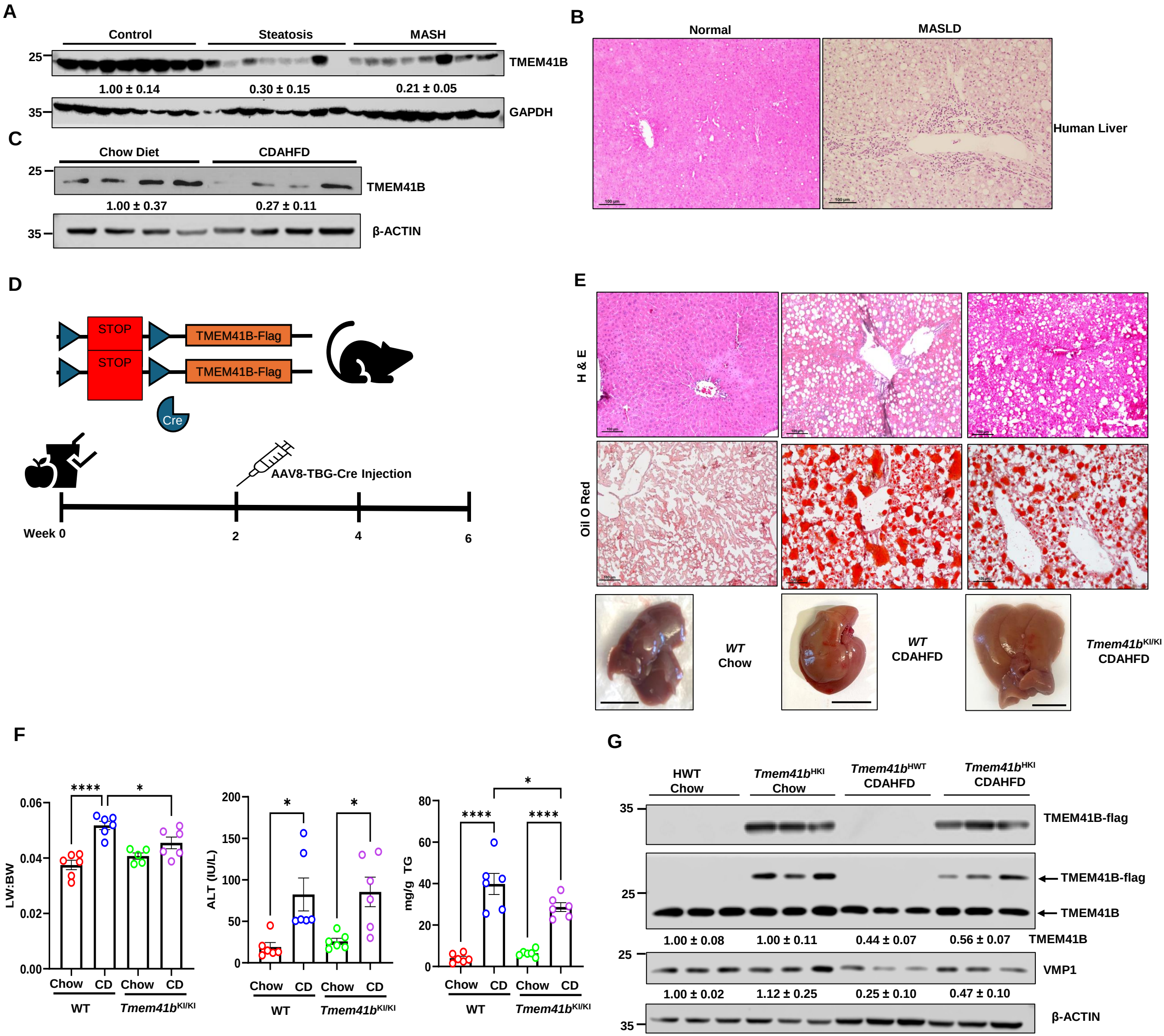
A
Control
Steatosis
MASH
25
TMEM41B
1.00 ± 0.14
0.30 ± 0.15
0.21 ± 0.05
35
GAPDH
B
Normal
MASLD
Human Liver
C
Chow Diet
CDAHFD
25
TMEM41B
1.00 ± 0.37
0.27 ± 0.11
35
β-ACTIN
D
STOP
STOP
TMEM41B-Flag
TMEM41B-Flag
Cre
AAV8-TBG-Cre Injection
Week 0
2
4
6
E
H & E
Oil O Red
WT
Chow
WT
CDAHFD
Tmem41b KI/KI
CDAHFD
F
LW:BW
ALT (IU/L)
mg/g TG
Chow
CD
WT
Tmem41b KI/KI
G
HWT
Chow
Tmem41b HKI
Chow
Tmem41b HWT
CDAHFD
Tmem41b HKI
CDAHFD
TMEM41B-flag
TMEM41B-flag
TMEM41B
1.00 ± 0.08
1.00 ± 0.11
0.44 ± 0.07
0.56 ± 0.07
TMEM41B
VMP1
1.00 ± 0.02
1.12 ± 0.25
0.25 ± 0.10
0.47 ± 0.10
β-ACTIN

Figure 4

A

Blue: indicates values are significant lower p≤0.05

Red: indicates values are significant higher p≤0.05

No-color text and cell: mean values are not significantly different for that comparison

Pathway	Biochemical Name	*Tmem41b* ^{HKO}/*Tmem41b* ^{HWT}			*Vmp1* ^{HKO}/*Vmp1* ^{HWT}	
		1 week	2 weeks	4 weeks	1 week	2 weeks
PC Metabolism	Phosphotidylcholine (PC)	1.06	0.99	**0.81**	**0.83**	**0.73**
	Lysophosphotidylcholine (LPC)	**0.72**	**0.51**	**0.4**	**0.49**	**0.35**
	choline	**0.76**	**0.66**	**0.64**	**0.66**	0.87
	choline phosphate	1.01	**2.33**	**2.69**	**2.69**	**3.01**
	cytidine 5'-diphosphocholine	**0.6**	**0.49**	**0.3**	**0.7**	**0.54**
PE Metabolism	Phosphotidylethanolamine (PE)	0.98	**0.8**	**0.5**	**0.68**	**0.41**
	Lysophosphotidylethanolamine (LPE)	0.83	**0.61**	**0.33**	**0.61**	**0.35**
	phosphoethanolamine	**0.69**	**0.73**	0.95	**0.78**	**1.29**
	cytidine-5'-diphosphoethanolamine	**0.69**	**0.58**	**0.39**	**0.63**	**0.38**
Neutral Lipids	Cholesteryl Esters	**5.16**	**11.24**	**23.77**	**7.49**	**14.47**
	Diacylglycerols (DAG)	**3.9**	**7.34**	**16.02**	**2.9**	**9.15**
	Triacylglycerols (TAG)	**4.82**	**15.47**	**24.48**	**9.54**	**18.54**
	Monoacylglycerols (MAG)	1.07	0.95	1.06	1.04	**1.95**

B

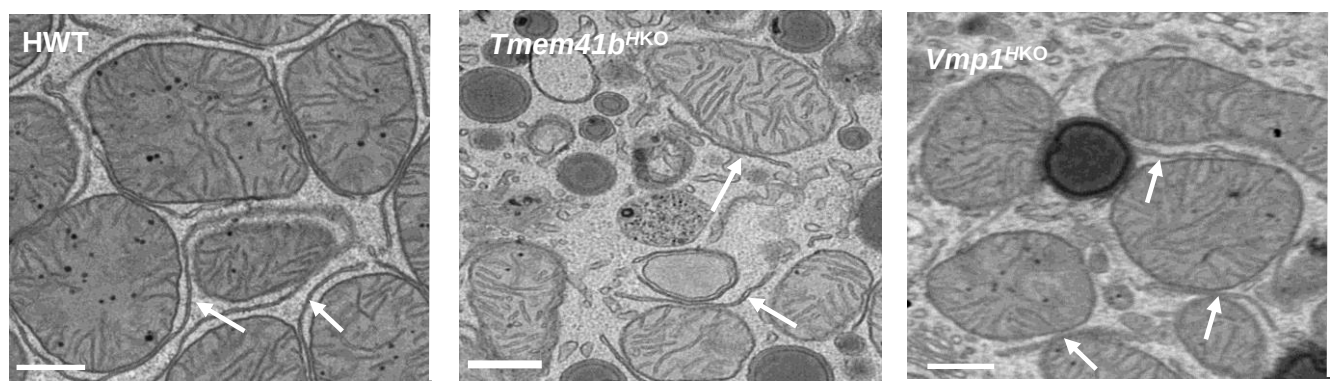

C

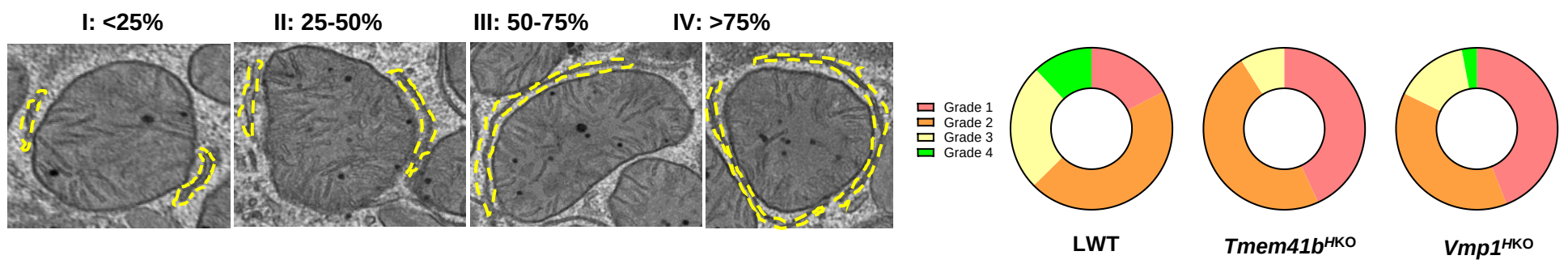

D

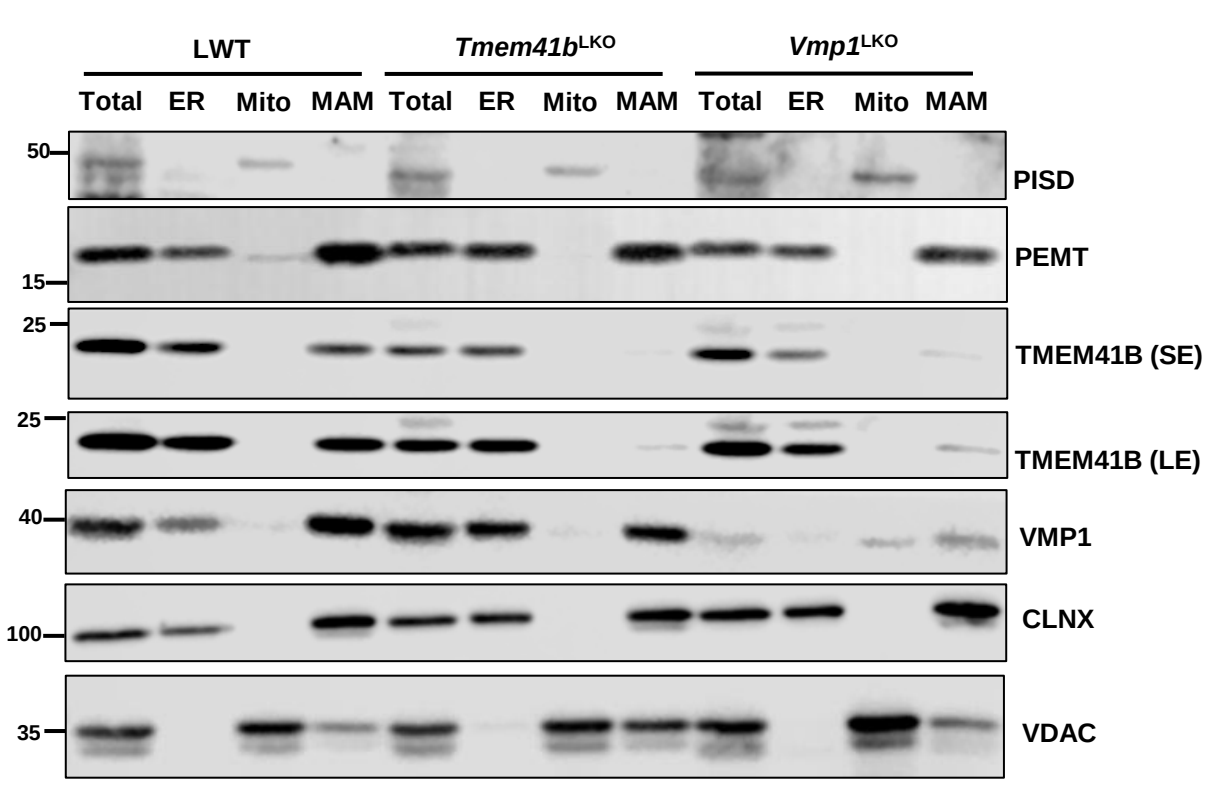

Figure 5

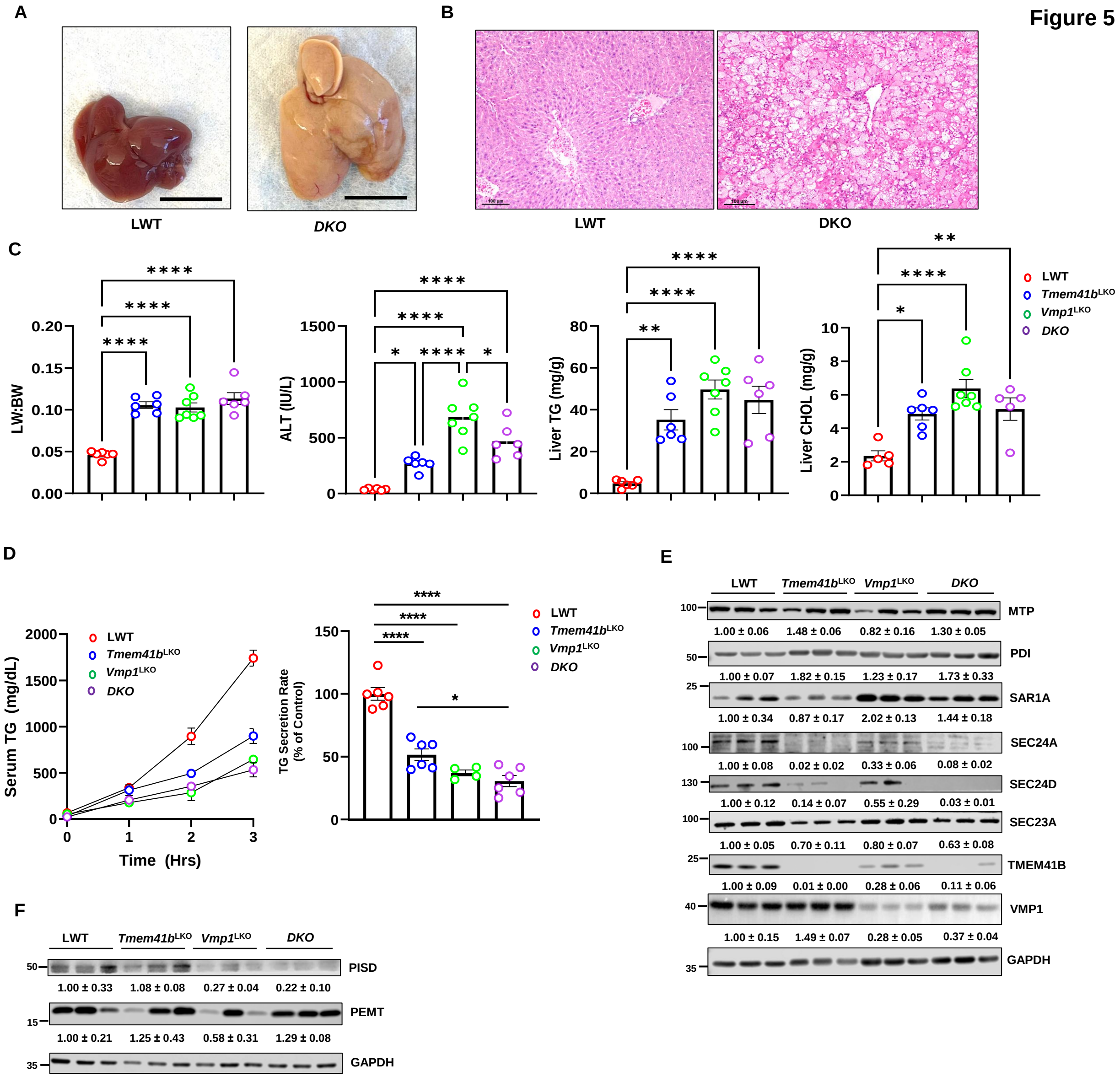
A
LWT
DKO
B
LWT
DKO
C
LW:BW
ALT (IU/L)
Liver TG (mg/g)
Liver CHOL (mg/g)
LWT
Tmem41b LKO
Vmp1 LKO
DKO
D
Serum TG (mg/dL)
Time (Hrs)
TG Secretion Rate (% of Control)
E
MTP
1.00 ± 0.06 1.48 ± 0.06 0.82 ± 0.16 1.30 ± 0.05
PDI
1.00 ± 0.07 1.82 ± 0.15 1.23 ± 0.17 1.73 ± 0.33
SAR1A
1.00 ± 0.34 0.87 ± 0.17 2.02 ± 0.13 1.44 ± 0.18
SEC24A
1.00 ± 0.08 0.02 ± 0.02 0.33 ± 0.06 0.08 ± 0.02
SEC24D
1.00 ± 0.12 0.14 ± 0.07 0.55 ± 0.29 0.03 ± 0.01
SEC23A
1.00 ± 0.05 0.70 ± 0.11 0.80 ± 0.07 0.63 ± 0.08
TMEM41B
1.00 ± 0.09 0.01 ± 0.00 0.28 ± 0.06 0.11 ± 0.06
VMP1
1.00 ± 0.15 1.49 ± 0.07 0.28 ± 0.05 0.37 ± 0.04
GAPDH
F
PISD
1.00 ± 0.33 1.08 ± 0.08 0.27 ± 0.04 0.22 ± 0.10
PEMT
1.00 ± 0.21 1.25 ± 0.43 0.58 ± 0.31 1.29 ± 0.08
GAPDH

Figure 6

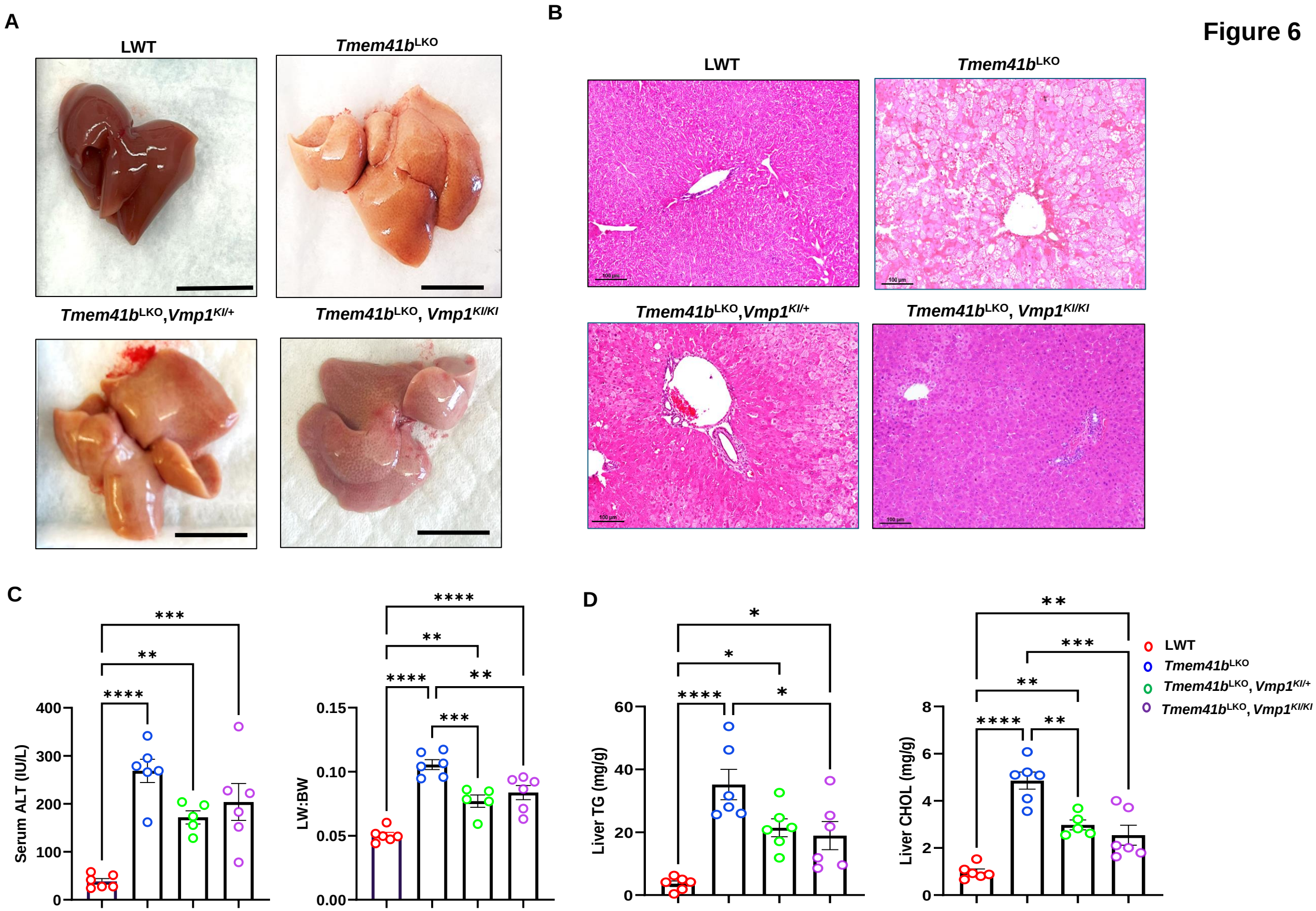
A
LWT
Tmem41b LKO
Tmem41b LKO,Vmp1 KI/+
Tmem41b LKO, Vmp1 KI/KI
B
LWT
Tmem41b LKO
Tmem41b LKO,Vmp1 KI/+
Tmem41b LKO, Vmp1 KI/KI
100 µm
C
Serum ALT (IU/L)
LW:BW
D
Liver TG (mg/g)
Liver CHOL (mg/g)
LWT
Tmem41b LKO
Tmem41b LKO, Vmp1 KI/+
Tmem41b LKO, Vmp1 KI/KI

Figure 7

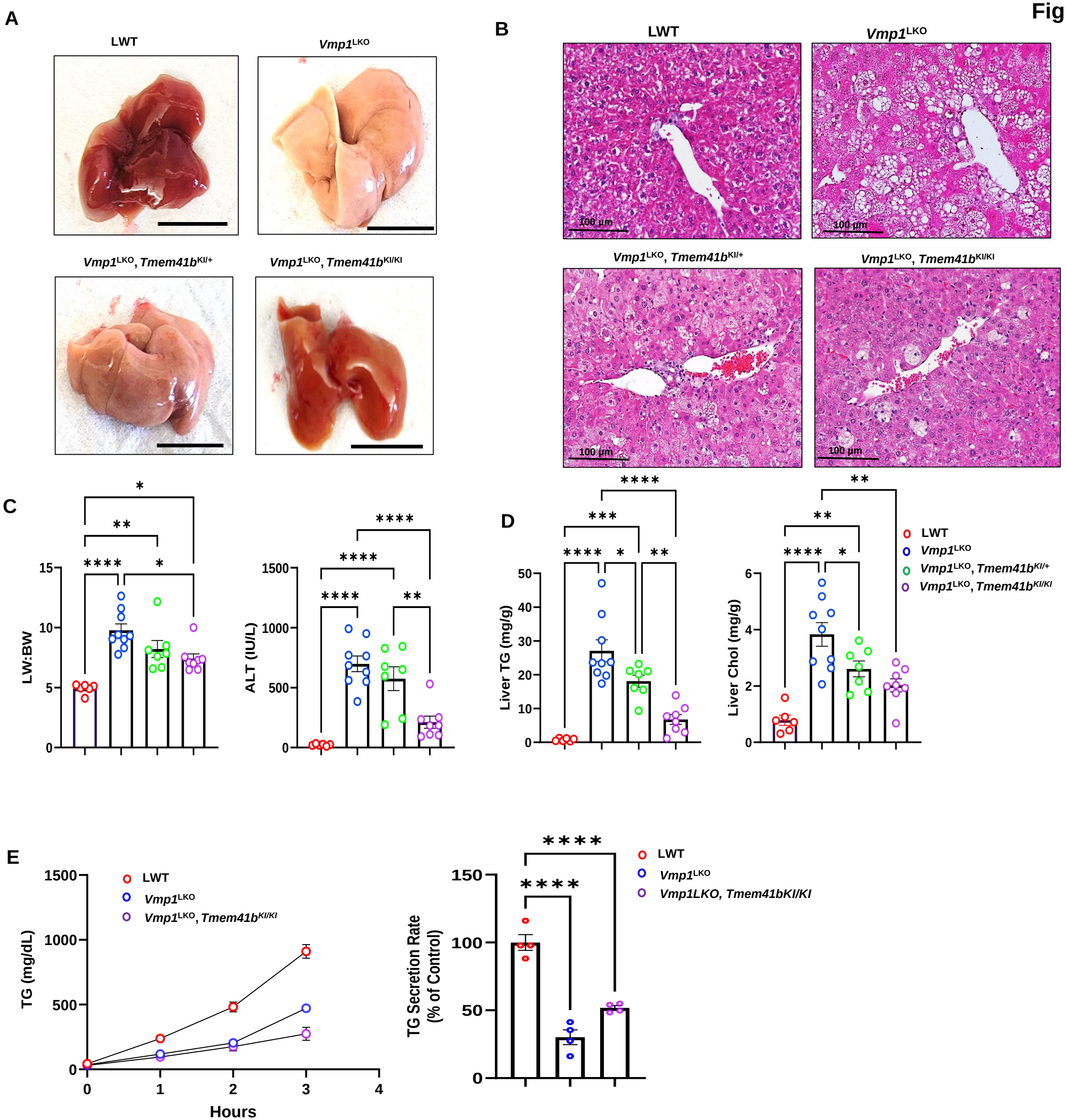
A
LWT
Vmp1LKO
Vmp1LKO, Tmem41bKI/+
Vmp1LKO, Tmem41bKI/KI
B
LWT
Vmp1LKO
Vmp1LKO, Tmem41bKI/+
Vmp1LKO, Tmem41bKI/KI
100 µm
C
LW:BW
ALT (IU/L)
D
Liver TG (mg/g)
Liver Chol (mg/g)
LWT
Vmp1LKO
Vmp1LKO, Tmem41bKI/+
Vmp1LKO, Tmem41bKI/KI
E
TG (mg/dL)
Hours
LWT
Vmp1LKO
Vmp1LKO, Tmem41bKI/KI
TG Secretion Rate (% of Control)
LWT
Vmp1LKO
Vmp1LKO, Tmem41bKI/KI

Figure 8

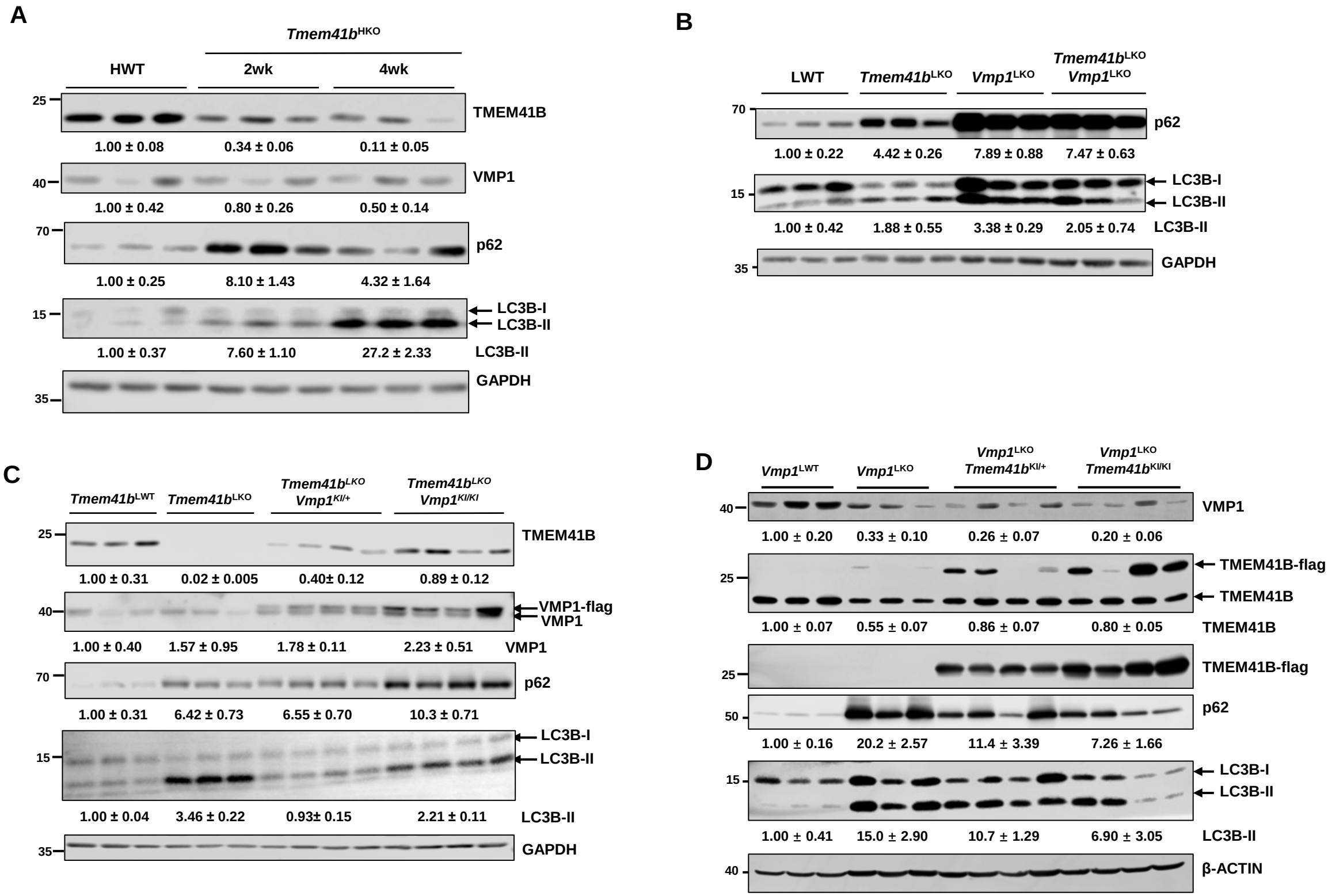
A
Tmem41b HKO
HWT
2wk
4wk
25
TMEM41B
1.00 ± 0.08
0.34 ± 0.06
0.11 ± 0.05
40
VMP1
1.00 ± 0.42
0.80 ± 0.26
0.50 ± 0.14
70
p62
1.00 ± 0.25
8.10 ± 1.43
4.32 ± 1.64
15
LC3B-I
LC3B-II
1.00 ± 0.37
7.60 ± 1.10
27.2 ± 2.33
LC3B-II
35
GAPDH
B
LWT
Tmem41b LKO
Vmp1 LKO
Tmem41b LKO Vmp1 LKO
70
p62
1.00 ± 0.22
4.42 ± 0.26
7.89 ± 0.88
7.47 ± 0.63
15
LC3B-I
LC3B-II
1.00 ± 0.42
1.88 ± 0.55
3.38 ± 0.29
2.05 ± 0.74
LC3B-II
35
GAPDH
C
Tmem41b LWT
Tmem41b LKO
Tmem41b LKO Vmp1 KI/+
Tmem41b LKO Vmp1 KI/KI
25
TMEM41B
1.00 ± 0.31
0.02 ± 0.005
0.40± 0.12
0.89 ± 0.12
40
VMP1-flag
VMP1
1.00 ± 0.40
1.57 ± 0.95
1.78 ± 0.11
2.23 ± 0.51
VMP1
70
p62
1.00 ± 0.31
6.42 ± 0.73
6.55 ± 0.70
10.3 ± 0.71
15
LC3B-I
LC3B-II
1.00 ± 0.04
3.46 ± 0.22
0.93± 0.15
2.21 ± 0.11
LC3B-II
35
GAPDH
D
Vmp1 LWT
Vmp1 LKO
Vmp1 LKO Tmem41b KI/+
Vmp1 LKO Tmem41b KI/KI
40
VMP1
1.00 ± 0.20
0.33 ± 0.10
0.26 ± 0.07
0.20 ± 0.06
25
TMEM41B-flag
TMEM41B
1.00 ± 0.07
0.55 ± 0.07
0.86 ± 0.07
0.80 ± 0.05
TMEM41B
25
TMEM41B-flag
50
p62
1.00 ± 0.16
20.2 ± 2.57
11.4 ± 3.39
7.26 ± 1.66
15
LC3B-I
LC3B-II
1.00 ± 0.41
15.0 ± 2.90
10.7 ± 1.29
6.90 ± 3.05
LC3B-II
40
β-ACTIN

Supplementary Table 1. List of antibodies and reagents used in the study.

1.1 Antibodies

Name	Citation	Supplier	Cat no.	Clone no.
anti-APOB (rabbit polyclonal)	PMID: 33445170	Washington U. (Dr. Nicholas Davidson)		
anti-Calnexin (rabbit polyclonal)		Santa Cruz Biotecchnology	sc-11397	
anti-F4/80 (rat monoclonal)		Invitrogen	14-4801-85	BM8
anti-FLAG (mouse monoclonal)		Sigma-Aldrich	F3165	M2
anti-GAPDH (rabbit monoclonal)		Cell Signaling Technology	2118	14C10
anti-LC3 (rabbit polyclonal)	PMID: 27151180			
anti-MTP (mouse monoclonal)		Santa Cruz Biotecchnology	sc-135994	8
anti-p62 (mouse monoclonal)		Abnova	H00008878	M01
anti-PEMT (rabbit polyclonal)		ThermoFisher	PIPA542383	
anti-PDI (rabbit polyclonal)		Sigma-Aldrich	P7372	
Anti-PISD (rabbit polyclonal)		Proteintech	16401-1-AP	
anti-SAR1A (rabbit polyclonal)		Proteintech	15350-1-AP	
anti-SEC23A (rabbit polyclonal)		Cell Signaling Technology	8162	
anti-SEC24C (rabbit polyclonal)		Cell Signaling Technology	8531	
anti-SEC24D (rabbit monoclonal)		Cell Signaling Technology	14687	D9M7L
anti-TMEM41B (rabbit polyclonal)		Proteintech	29270-1-AP	
anti-TMEM41B (rabbit polyclonal)		Sigma-Aldrich	HPA014946	
anti-VMP1 (rabbit monoclonal)		Cell Signaling Technology	12929	D1Y3E
anti-α-SMA (rabbit polyclonal)		Abcam	ab5694	
anti-β-actin (mouse monoclonal)		Sigma-Aldrich	A5441	AC-15
anti-VDAC (rabbit polyclonal)		Calbiochem	AB10527	
HRP-goat anti-rabbit		Jackson Immuno Research	111-035-144	

HRP-goat anti-mouse		Jackson Immuno Research	115-035-146	
HRP-goat anti-rat		Jackson Immuno Research	112-035-143	
HRP-goat anti-rat		Vector Laboratories	MP-7444	

1.2 Organisms

Name	Citation	Supplier	Strain	Sex	Age	Overall number
Tmem41b^{flox}		This paper		Males and females	8-10 weeks	
Tmem41b^{Ki}		This paper		Males and females	8-10 weeks	
Vmp1^{flox}		The European Mouse Mutant Archive	EM:05506	Males and females	8-10 weeks	
Vmp1^{KI}		This paper		Males and females	8-10 weeks	
Tmem41b^{flox} *Vmp1*^{flox}		This paper		Males and females	8-10 weeks	
Vmp1^{flox} *Tmem41b*^{KI}		This paper		Males and females	8-10 weeks	
Alb-cre		Jackson Laboratory	#003574	Males and females	8-10 weeks	
Tmem41b^{flox} *Vmp1*^{KI}		This paper		Males and females	8-10 weeks	

1.3 Sequence based reagents

Name	Forward (5' – 3')	Reverse (5' – 3')
Acta2	CCACCGCAAATGCTTCTAAGT	GGCAGGAATGATTTGGAAAGG
Actb	TGTTACCAACTGGGACGACA	GGGGTGTTGAAGGTCTCAAA
Adgre	CTTTGGCTATGGGCTTCCAGTC	GCAAGGAGGACAGAGTTTATCGTG
Cd68	TGCGGCTCCCTGTGTGT	TCTTCCTCTGTTCCTTGGGCTAT
Col1a1	TGTGTTCCCTACTCAGCCGTCT	CATCGGTCATGCTCTCTCCAA
Ctgf	CTGCCAGTGGAGTTCAAATGC	TCATTGTCCCCAGGACAGTTG

Il1b	GCCCATCCTCTGTGACTCAT	AGGCCACAGGTATTTTGTCG
Il10	CCAAGCCTTATCGGAAATGA	TTTTCACAGGGGAGAAATCG
Tgfb1	TGCTAATGGTGGACCGCAA	CACTGCTTCCCGAATGTCTGA
Trem2	TATGACGCCTTGAAGCACTG	AGAGTGATGGTGACGGTTCC

1.4 Biological samples

Description	Source	Identifier
Human liver samples	University of Kansas Medical Center	

1.5 Software

Software name	Manufacturer	Version
GraphPad	Prism	Ver 9.0
Image J	NIH/Macintosh	ImageJ2
SigmaPlot	Systat Software	Version 12
Un-Scan-It	Silk Scientific	Version 6.1

1.6 Other (e.g. drugs, proteins, vectors etc.)

Name	Supplier	Cat no.
AAV8-TBG-iCre	Vector Biolabs	
AAV8-TBG-null	Vector Biolabs	
ALT (SGPT) liquid reagents	Pointe Scientific	A7526
CDAHFD	Research Diet	A6071309
Cholesterol liquid reagents	Pointe Scientific	C7510
Oil red O	Sigma-Aldrich	O0625
Pluronic F-127	Thermo Fisher	p6866
Ponceau S	Sigma-Aldrich	P3504
Protease inhibitor cocktail	Bimake	B14002
2xSYBR Green qPCR Master Mix	Bimake	B21202
Triglycerides liquid reagents	Pointe Scientific	T7532
Trizol reagent	Thermo Fisher	
HiMark™ prestained protein standard	ThermoFisher Scientific	LC5699
PageRuler™ prestained protein ladder	ThermoFisher Scientific	PI26617

Supplementary Figure Legends

Supplementary Fig. 1. Hepatic deletion of TMEM41B impairs lipoprotein secretion and leads to rapid development of a micro-vesicular steatosis in mice. (A) Representative images of 1-month-old *Tmem41b*^{LKO} and matched WT mice and liver-body weight ratio. (B) H&E staining of liver tissues from LWT and *Tmem41b*^{LKO} mice. Scale bars, 100 µm. Hepatic (C) and serum (D) TG and cholesterol (CHOL) were quantified. (E) LWT and *Tmem41b*^{LKO} mice were injected with Pluronic™ F-127 and serum TG concentrations were measured. TG secretion rate bars, 100 µm. Hepatic (C) and serum (D) TG and cholesterol (CHOL) were quantified. (E) LWT and *Tmem41b*^{LKO} mice were injected with Pluronic™ F-127 and serum TG concentrations were measured. TG secretion rate was quantified. Serum APOB from LWT and *Tmem41b*^{LKO} mice were subjected to immunoblot analysis. (F) Serum ALT activities were measured in 1-month-old *Tmem41b*^{LKO} and matched WT mice. Statistical analyses were performed by t-test. ***p<0.001, ****p<0.0001 (unpaired Student's *t test*).

Supplementary Fig. 2. Hepatic deletion of TMEM41B impairs lipoprotein secretion and leads to rapid development of a micro-vesicular steatosis in female mice. (A) Liver/Body Weight ratio in 8-10 weeks old *Tmem41b* ^{flox} female mice at 2 weeks post AAV8-TBG-cre injection. Hepatic (B-C) and serum (D-E) TG and cholesterol were measured in female mice fed ad libitum of a chow diet. (F) Serum ALT activities were measured in *Tmem41b* ^{flox} female mice at 2 weeks post AAV8-TBG-cre injection. * p<0.05; *** p < 0.001; ****p<0.0001 (unpaired Student's *t test*).

Figure S1

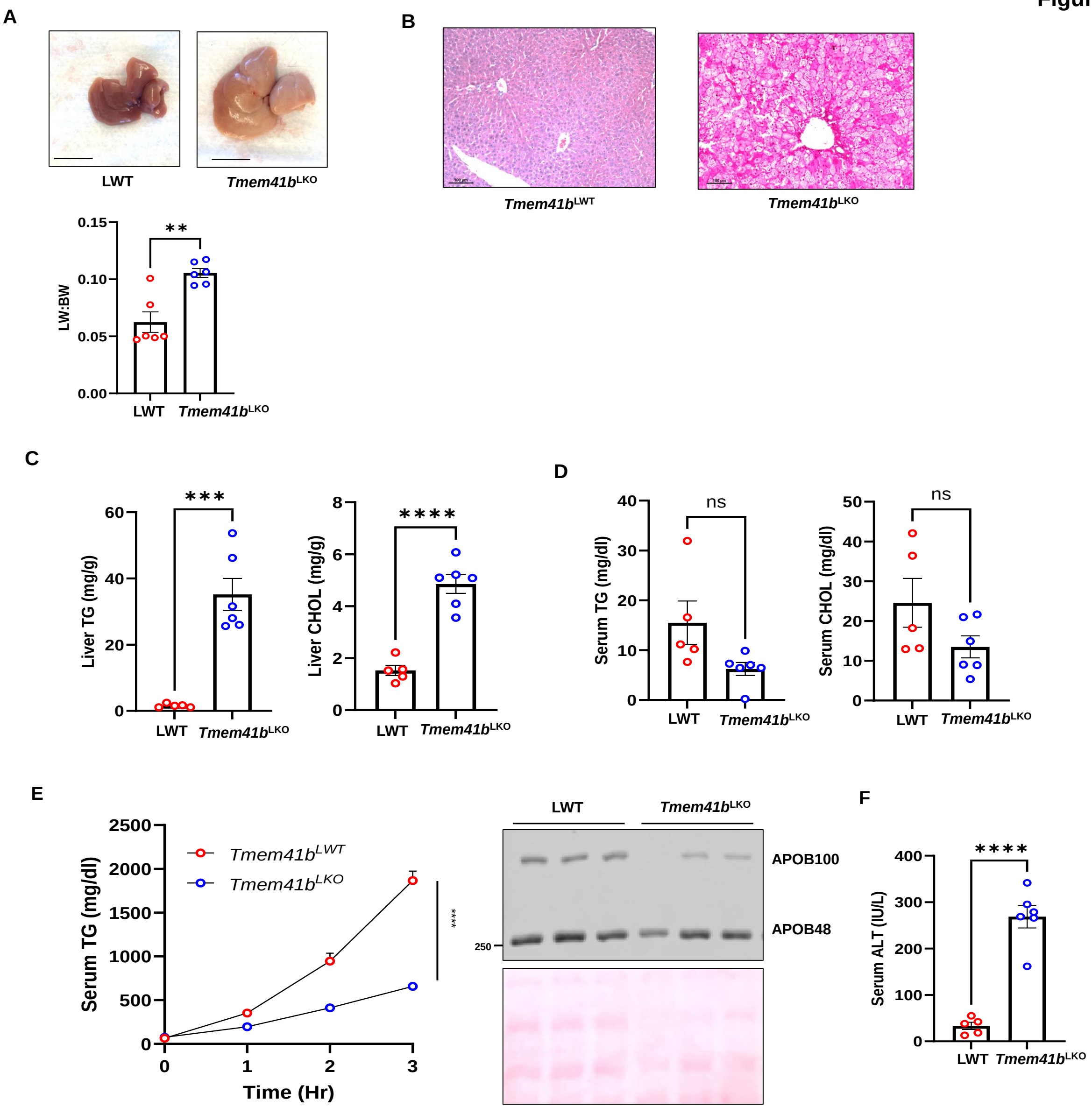
A
LWT
Tmem41b^LKO
B
Tmem41b^LWT
Tmem41b^LKO
LW:BW
0.15
0.10
0.05
0.00
**
LWT
Tmem41b^LKO
C
Liver TG (mg/g)
60
40
20
0
***
LWT
Tmem41b^LKO
Liver CHOL (mg/g)
8
6
4
2
0
****
LWT
Tmem41b^LKO
D
Serum TG (mg/dl)
40
30
20
10
0
ns
LWT
Tmem41b^LKO
Serum CHOL (mg/dl)
50
40
30
20
10
0
ns
LWT
Tmem41b^LKO
E
Serum TG (mg/dl)
2500
2000
1500
1000
500
0
Tmem41b^LWT
Tmem41b^LKO
****
0
1
2
3
Time (Hr)
LWT
Tmem41b^LKO
APOB100
APOB48
250
F
Serum ALT (IU/L)
400
300
200
100
0
****
LWT
Tmem41b^LKO

Figure S2

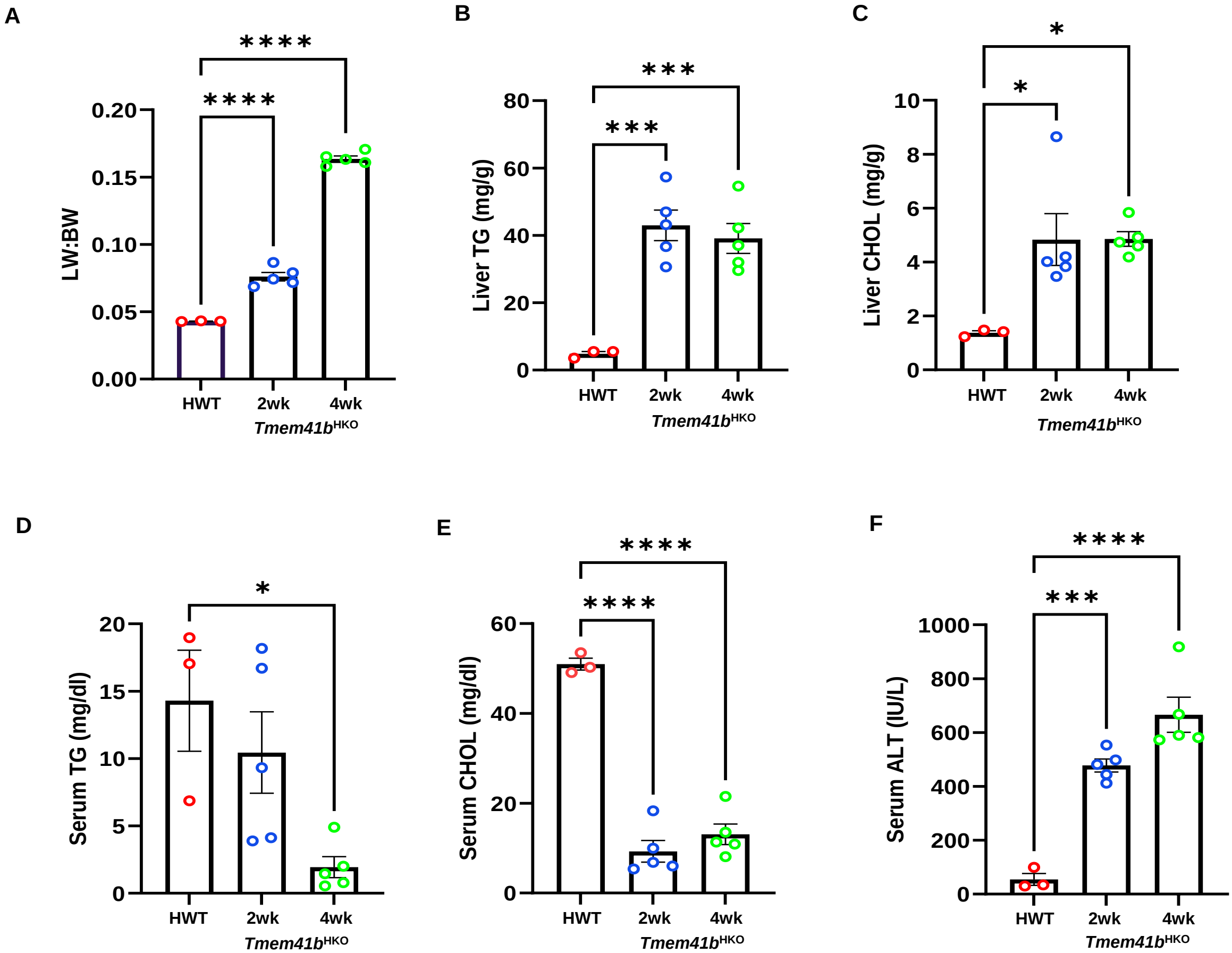
A
****
****
LW:BW
0.20
0.15
0.10
0.05
0.00
HWT
2wk
4wk
Tmem41b HKO
B
***
***
Liver TG (mg/g)
80
60
40
20
0
HWT
2wk
4wk
Tmem41b HKO
C
*
*
Liver CHOL (mg/g)
10
8
6
4
2
0
HWT
2wk
4wk
Tmem41b HKO
D
*
Serum TG (mg/dl)
20
15
10
5
0
HWT
2wk
4wk
Tmem41b HKO
E
****
****
Serum CHOL (mg/dl)
60
40
20
0
HWT
2wk
4wk
Tmem41b HKO
F
****
***
Serum ALT (IU/L)
1000
800
600
400
200
0
HWT
2wk
4wk
Tmem41b HKO